



NIH Public Access

Author Manuscript

Chem Mater. Author manuscript; available in PMC 2013 July 10.

Published in final edited form as:
Chem Mater. 2012 July 10; 24(13): 2472–2485. doi:10.1021/cm3004408.

Topological and Conformational Effects on Electron Transfer Dynamics in Porphyrin-[60]Fullerene Interlocked Systems

Jackson D. Megiatto Jr.[§], David I. Schuster[§], Gustavo de Miguel^{‡,†}, Silke Wolfrum[‡], and Dirk M. Guldi[‡]

Jackson D. Megiatto: jackson.megiatto@asu.edu; David I. Schuster: david.schuster@nyu.edu; Dirk M. Guldi: guldi@chemie.uni-erlangen.de

[§]Department of Chemistry, New York University, New York, NY 10003, USA

[‡]Department of Chemistry and Pharmacy and Interdisciplinary Center for Molecular Materials, Friedrich-Alexander-Universität Erlangen-Nürnberg, 91058 Erlangen, Germany

Abstract

The effect of molecular topology, and conformation on the dynamics of photoinduced electron transfer (ET) processes has been studied in interlocked electron donor-acceptor systems, specifically rotaxanes with zinc(II)-tetraphenylporphyrin (ZnP) electron donor and [60]fullerene (C_{60}) as the electron acceptor. Formation or cleavage of coordinative bonds was used to induce major topological and conformational changes in the interlocked architecture. In the first approach, the tweezers-like structure created by the two ZnP stopper groups on the thread was used as a recognition site for complexation of 1,4-diazabicyclo[2.2.2]octane (DABCO), which creates a bridge between the two ZnP moieties on the rotaxane, generating a catenane structure. The photoinduced processes in the DABCO-complexed $(ZnP)_2$ -[2]catenate- C_{60} system were compared with those of the $(ZnP)_2$ -rotaxane- C_{60} precursor and the previously reported ZnP-[2]catenate- C_{60} . Steady-state emission and transient absorption studies showed that a similar multistep ET pathway emerged for rotaxanes and catenanes upon photoexcitation at various wavelengths, ultimately resulting in a long-lived $ZnP^{•+}/C_{60}^{•-}$ charge separated radical pair state. However, the decay kinetics of the latter states clearly reflect the topological differences between the rotaxane, the catenane, and DABCO-complexed-catenate architectures. The lifetime of the long-distance $ZnP^{•+}-[Cu(I)phen_2]^{•+}-C_{60}^{•-}$ charge separated state is more than four times longer in **3** (1.03 μ s) than in **1** (0.24 μ s) and approaches that in catenane **2** (1.1 μ s). The results clearly showed that adoption of a catenane from a rotaxane topology inhibits the charge recombination process. In a second approach, the Cu(I) ion used as template to assemble the $(ZnP)_2$ - $[Cu(I)phen_2]^{•+}-C_{60}$ rotaxane was removed, and structural analysis suggested a major topographical change occurred, such that charge separation between the chromophores was no longer observed upon photoexcitation in nonpolar as well as polar solvents. Only ZnP and C_{60} triplet excited states were observed upon laser excitation. These results highlighted the critical importance of the central Cu(I) ion for long range ET processes in these large interlocked electron donor-acceptor systems.

Correspondence to: Jackson D. Megiatto, Jr., jackson.megiatto@asu.edu; David I. Schuster, david.schuster@nyu.edu; Dirk M. Guldi, guldi@chemie.uni-erlangen.de.

[†]Present address: Department of Physical Chemistry, University of Castilla-La Mancha, 45071 Toledo, Spain

Supporting Information. Experimental details for preparation as well as spectroscopic characterization of building blocks and synthetic intermediates. This material is available free of charge via the Internet at <http://pubs.acs.org>.

Keywords

Rotaxanes; Catenanes; Electron Transfer; Porphyrin; Fullerene

Introduction

Catenanes^{1,2} and rotaxanes^{3,4} are prime examples of supramolecular interactive scaffolds.^{5,6} Their inherent ability to undergo controlled motions that can be triggered by external stimuli makes these nanoscale systems very promising for various applications, including drug delivery,^{7–9} catalysis,^{10–12} polymers^{13–15}, molecular sensors^{16–18} and machines.^{19–21} Catenanes are composed of two or more interlocked rings, while rotaxanes are systems in which a ring is threaded by a rod to which two bulky terminal groups are attached to prevent dissociation.^{1–4} Topological and conformational changes in rotaxanes and catenanes are reflected in detectable responses that can be employed to probe electronic interactions among components of the interlocked system.^{22–26} In the field of artificial photosynthesis, the topological properties of rotaxanes^{27–35} and catenanes^{36–40} can be used to tune electronic interactions between appended electron donor (D) and acceptor (A) subunits in order to facilitate long-distance electron transfer (ET) processes and generate long-lived charge-separated states.

There is a significant literature on photoactive rotaxanes describing the effects of mechanical bonds on the photophysical properties of the D-A components.^{27–35} In these studies, minor structural modifications in the rotaxane structure, such as variation of the size and shape of the ring and thread components, were investigated regarding efficiency and kinetics of electron transfer (ET) processes. On the other hand, studies of the ET dynamics in the related D-A catenane architecture are quite rare.^{39,40} This difference can be attributed to the inherent synthetic difficulties that arise when preparing catenanes compared to those of more accessible rotaxanes. Thus, investigation of the effects of major topological changes on the photoinduced processes of D-A interlocked systems is extremely limited.

The only critical comparison between the photophysical properties of rotaxanes and catenanes was reported by Sauvage and coworkers.^{41,46} In their pioneering work, a large family of rotaxanes and catenanes assembled through formation of a central Cu(I)-(phenanthroline)₂ ([Cu(phen)₂]⁺) complex and bearing appended zinc(II)porphyrin (ZnP, the electron donor) and a gold(III)porphyrin (AuP, the electron acceptor) was prepared and their photophysical properties were investigated. Much insight into topological differences and ET dynamics was afforded. Unfortunately, overlapping of the spectroscopic signals as well as ultrafast charge recombination processes prohibited the determination of the kinetic parameters for many of the intermediates formed upon excitation of these systems.

Inspired by the work of Sauvage and colleagues,^{41–46} we have designed and prepared analogous [Cu(phen)₂]⁺ based rotaxanes and catenanes bearing ZnP as the electron donor, but with C₆₀ as the ultimate electron acceptor in place of AuP.^{47–50} The choice of C₆₀ is grounded on its extraordinary redox and spectroscopic properties,^{51,52} which have allowed determination of rates of formation and decay of electronically excited and charge separated states that were impossible to obtain in the previous purely porphyrinic interlocked systems.

Our recent synthetic achievements^{53–57} in the field of interlocked systems have allowed the efficient preparation of rotaxane **1**⁵⁸ and catenate **2**^{59,60} (Figure 1), for which key structural parameters are identical, including the size and shape of the ring and thread components as well as the connecting groups that link the ZnP and C₆₀ moieties to the interlocked structure. The only and critical difference between the two systems is their distinct topology.

Consequently, rotaxane **1** and catenate **2** are ideal systems for the investigation of topological effects on ET dynamics.

A complete molecular characterization of the structures shown in Figure 1 indicates that rotaxane **1** is highly flexible and folds to form a compact structure in solution as a consequence of secondary attractive intramolecular interactions between the chromophores.⁵⁸ On the other hand, in the more rigid catenate **2** these attractive interactions are not strong enough to bring the chromophores close to each other, resulting in an extended conformation with the ZnP and C₆₀ groups at opposite ends of the system.⁵⁷ A detailed photophysical investigation confirmed the stretched conformation for catenate **2**, reflecting the relative rigidity of its structure.⁵⁹

In this contribution, we report on the photophysical properties of rotaxane **1** to compare with those of the [2]catenate **2**. It was found that the folded molecular structure of flexible rotaxane **1** causes major effects on the ET dynamics, resulting in quite different rates for the decay of the charge separated states when compared to those of the catenate **2**. Our data suggest that the higher flexibility of the rotaxane structure allows reorientation of the chromophores to afford molecular conformations that are not available in the more rigid [2]catenate assembly, resulting in distinct photophysical dynamics.

To confirm this hypothesis, we explored two strategies based on formation and cleavage of two different types of intramolecular coordinative bonds to promote major changes in the flexibility of the molecular architecture of prototype rotaxane **1**. In the first approach, designed to reduce conformational flexibility, we harnessed the well-known ability of ZnP groups in **1** to interact ($K_d = 10^5 - 10^8$),^{49,61-67} with the bidentate ligand 1,4-diazabicyclo[2.2.2]octane (DABCO) to change the topology of the system from a rotaxane to a catenane. The rotaxane to catenane topological change induced by intramolecular coordination with a single DABCO molecule brought the two ZnP groups close to each other (as depicted in compound **3**, Figure 2), significantly reducing the flexibility of **1**.

The second strategy was designed to increase the flexibility of the rotaxane structure by removing the Cu(I) template ion from the [Cu(phen)₂]⁺ complex core. Removal of the Cu(I) template ion is expected to cause a significant change in the photophysical processes of rotaxanes, as a result of reorientation of the chromophores in the more flexible demetalated interlocked structure, analogous to that seen in previous works.^{46,68,69} Accordingly, the Cu-free rotaxane **4** (Figure 2) was prepared, and its photophysical properties were investigated. We were then able to critically compare the thermodynamic and kinetic parameters of the EnT and ET processes of rotaxane **1**, DABCO-bridging catenate **3** and Cu-free rotaxane **4** with each other and with those previously reported for the related [2]catenate **2**.⁵⁹

Experimental Section

General Information and Materials

NMR spectra were obtained on a Bruker AVANCE 400 (400 MHz) spectrometer using deuterated solvents as the lock. The spectra were collected at 25 °C and chemical shifts (δ , ppm) were referenced to residual solvent peak (¹H, CDCl₃ at 7.26 ppm). In the assignments, the chemical shift (in ppm) is given first, followed, in brackets, by multiplicity (s, singlet; d, doublet; t, triplet; m, multiplet; br, broad), the value of the coupling constants in Hz if applicable, the number of protons implied and finally the assignment. In the ¹H NMR assignment (δ), H_o and H_m refer to the hydrogen atoms at the *ortho* and *meta* positions, respectively, of the phenyl ring attached to the phenanthroline ring system, whose hydrogen atoms are numbered H_{3,8}, H_{4,7}, H_{5,6}, respectively. Ar is used as an abbreviation for aromatic ring. MALDI-TOF mass spectra were recorded in a Bruker OmniFLEX MALDI-TOF MS

Spectrometer. This instrument was operated at an accelerating potential of 20 kV in linear mode. The mass spectra represent an average over 256 consecutive laser shots. The mass scale was calibrated using the matrix peaks and the calibration software available from Bruker OmniFLEX. Mentioned *m/z* values correspond to monoisotopic masses. The compound solutions (10^{-3} mol/L) were prepared in THF. The matrix material was purchased from Aldrich and used without further purification. The matrix, α -cyano-4-hydroxy-cinnamic acid (CCA), was dissolved (10 g/L) in a solvent mixture composed of H₂O/CH₃CN/TFA (25/75/1, v/v). Two microliters of compound solution was mixed with 10 μ L of matrix solution. The final solution was deposited onto the sample target and allowed to dry in air. All chemicals were purchased from Sigma-Aldrich, Alfa Aesar and Acros Organics and were used without further purification. For moisture sensitive reactions, solvents were freshly distilled. Methylene chloride (CH₂Cl₂) and acetonitrile (CH₃CN) were dried over calcium hydride while tetrahydrofuran (THF) was dried using sodium/benzophenone. Anhydrous dimethylformamide (DMF) was used as received. All syntheses were carried out using Schlenk-line techniques. Moisture sensitive liquids were transferred by canula or syringe. The progress of the reactions was monitored by thin-layer chromatography (TLC) whenever possible. TLC was performed using precoated glass plates (Silica gel 60, 0.25 mm thickness) containing a 254 nm fluorescent indicator. Column chromatography was carried out using Merck Silica gel 60 (0.063 – 0.200 mm). Rotaxane **1**,⁵⁸ catenate **2**,⁵⁹ DABCO-complexed catenane **3**,^{49,61–67} macrocycle **5**,⁵⁵ thread **6**,^{55,56} 4-ethylphenyl-tri(3,5-di-*tert*-butylphenyl)zinc(II)porphyrin^{58,59} and model compounds⁵⁹ **10**, **11** and **12** were synthesized following literature procedures.

Electrochemical and Photophysical Studies

All solvents used were spectroscopic grade (99.5%) and were purchased from Sigma-Aldrich. The samples were placed in fluorimetric cuvettes with different pathways and, when necessary, purged with oxygen or with argon. A single-compartment, three-electrode cell configuration was used in this work. A glassy carbon electrode (3 mm diameter) was used as the working electrode, a platinum wire as the counter, and an Ag wire as the reference electrode. All electrochemical measurements were performed with a E.G.C. Princeton Applied Research model 263A potentiostat/galvanostat. Femtosecond transient absorption studies were performed with 387 and 420 nm laser pulses (1 kHz, 150 fs pulse width) from an amplified Ti:Sapphire laser system (Model CPA 2101, Clark-MXR Inc.). Nanosecond Laser Flash Photolysis experiments were performed with 355 or 532 nm laser pulses from a Quanta-Ray CDR Nd:YAG system (6 ns pulse width) in a front face excitation geometry. Fluorescence lifetimes were measured by using a Fluorolog (Horiba Jobin Yvon). Steady-state fluorescence measurements were performed by using a Fluoromax 3 (Horiba Jobin Yvon). The experiments were performed at room temperature.

Synthesis of Rotaxane **9**

In flask A, macrocycle **5**⁵⁵ (0.056 g, 0.076 mmol) was dissolved in 2.0 mL of degassed DCM/CH₃CN (7:3, v/v) to which [Cu(CH₃CN)₄][PF₆] (0.028 g, 0.076 mmol) was added under N₂ and the solution was stirred at rt for 30 min. The azidophenanthroline ligand **6**⁵⁶ (0.052 g, 0.076 mmol) was then added as a solid to flask A and the deep red solution was stirred under N₂ at rt for 3 h to generate precursor **7**. Meanwhile, in the reaction flask, CuI (0.026 g, 0.137 mmol), sodium ascorbate (0.110 g, 0.548 mmol) and sulphonated bathophenanthroline^{53,59} (0.161 g, 0.274 mmol) were dissolved in 5 mL of degassed aqueous ethanol (1:1, v/v). The pink suspension was heated at reflux for 2 min and cooled back to rt. The deep red solution in the flask A containing **7** was then added by syringe to the reaction flask. Finally, 4-ethylphenyl-tri(3,5-di-*tert*-butylphenyl)zinc(II)porphyrin⁵⁹ (0.239 g, 0.23 mmol), dissolved in 4 mL of degassed DCM, and DBU (0.035 g, 0.34 μ L, 0.23 mmol) were added and the resulting purple mixture was stirred under nitrogen for 12 h

at rt. The crude mixture was extracted with DCM (3×50 mL). The organic phase was washed with distilled water (3×100 mL), concentrated to a volume of 10 mL and then stirred for 3 h with a saturated KPF₆ methanol solution to effect the anion exchange. The solvents were evaporated under reduced pressure; the remaining insoluble purple solid was extracted with DCM (3×100 mL) and filtered through paper. The filtrate was evaporated under reduced pressure and the crude product was purified by column chromatography (SiO₂) using DCM/CH₃OH (98/2 v/v) as eluent, affording rotaxane **8** (0.173 g, ~65%) as a purple solid, which was characterized by MALDI-TOF (*m/z* found 3544.69 [M – PF₆]⁺, calculated, 3544.58 for C₂₁₉H₂₃₂N₁₈O₁₅CuZn₂). Rotaxane **8** (0.053 g, 0.015 mmol) was dissolved in 10 mL of DCM/CH₃CN (3:2 v/v) to which was added a solution of KCN (0.020 g, 0.30 mmol) dissolved in 5 mL of H₂O, and the mixture was stirred at room temperature for 4 h. The organic layer was separated. The aqueous phase was extracted with DCM (3×50 mL). The combined organic layers were washed with distilled water (3×250 mL), dried over Na₂SO₄, filtered through paper and evaporated to dryness. Final purification was achieved by column chromatography (SiO₂) using DCM/CH₃OH (99/1 v/v) as eluent, affording **9** as a purple solid in quantitative yield (0.052 g). ¹H NMR (CDCl₃), δ ppm: 9.18 (s, 1H, CHO); 9.10-8.70 (m, 16H, pyrrolic protons) 8.30 (d, 4H, H_o); 8.20 (m, 4H, H_{4'}, H_{7'}, H₄, H₇); 8.16 (d, 4H, H_o); 8.10 (s, 2H, H-triazole rings) 8.07 (s, 12H, H_o of ZnP-*t*-butyl-*meso*Ar), 7.76 (dd, 8H, H of ZnP-*meso*Ar); 7.70 - 7.60 (m, 8H, H_{5'}, H_{6'}, and H_p of ZnP-*t*-butyl-*meso*Ar); 7.40 - 7.60 (dd, 4H, H_{3'}, H_{8'}, H₃, H₈); 6.90-7.10 (m, 8H, H_m and H_{m'}); 6.45 (s, 2H, H_o of benzaldehyde ring); 6.40 (d, 1H, H_p of benzaldehyde ring); 5.40 (s, 2H, H₅ and H₆); 4.50-2.80 (br, 48H, O-CH₂-CH₂-O); 1.54 (s, 108H, *tert*-butyl groups). MALDI-TOF: *m/z* found 3482.12 [M + H]⁺, calculated, 3481.70 for C₂₁₉H₂₃₂N₁₈O₁₅Zn₂.

Synthesis of Rotaxane 4

Precursor **9** (0.030 g, 8.6 μmol), C₆₀ (0.092 g, 0.129 mmol) and sarcosine (0.015, 0.172 mmol) were dissolved in 100 mL of toluene at room temperature using sonication and under an N₂ atmosphere. After 30 min, the reaction mixture was heated at reflux for 6 h under N₂ and magnetic stirring. The solvent was evaporated under reduced pressure, the crude product was dissolved in CH₂Cl₂ (50 mL) and washed with distilled water (3× 50 mL). The organic layer was dried over Na₂SO₄, filtered through paper and concentrated under reduced pressure. Final purification was achieved by successive column chromatography and preparative TLC (SiO₂) using CH₂Cl₂/MeOH (99:1, v/v) as eluant, to afford rotaxane **4** as a purple solid in 13% yield. ¹H NMR (CDCl₃), δ ppm: 9.10-8.80 (m, 16H, pyrrolic protons) 8.60-8.40 (m, 8H, H_o and H_{o'}); 8.40-8.20 (m, 4H, H_{4'}, H₄); 8.10-7.90 (m, 18H, H-triazole rings, H_o of ZnP-*t*-butyl-*meso*Ar and H_{5'}, H₅), 7.76 (m, 6H, H_p of ZnP-*meso*Ar); 7.20 - 6.90 (m, 17H, H_{m'}, H_{3'}, H₃, H_{o,p} of ZnP-*meso*-Ar and H_p of Ar ring on the macrocycle component); 6.82 (m, 2H, H_o of Ar ring on the macrocycle component); 6.71 (d, 4H, H_m); 6.50-6.20 (m, 3H, H of pyrrolidine ring); 5.50-3.00 (br, 51H, O-CH₂-CH₂-O and N-CH₃ on the pyrrolidine ring); 1.54 (s, 108H, *tert*-butyl groups). MALDI-TOF: *m/z* found 4229.60 [M + H]⁺, calculated, 4228.19 for C₂₈₁H₂₃₇N₁₉O₁₄Zn₂.

Results and Discussion

1 - Synthesis and Structural Characterization

1.1 - Rotaxane 1 and [2]catenate 2—Rotaxane **1** and catenate **2** were prepared and characterized as described previously.⁵³⁻⁵⁹ The conclusion that rotaxane **1** adopts a folded conformation in which one of the ZnP moieties is proximal to the [Cu(phen)₂]⁺ complex and the C₆₀ group, while the other ZnP moiety is further away, was based on ¹H NMR analysis and time-resolved fluorescence techniques, which clearly showed that the two ZnP groups in **1** were in different chemical/electronic environments.^{57,58} The same analysis indicated that

catenate **2** assumes a stretched conformation with the chromophores as far as possible from each other.^{57,59}

1.2 - DABCO-bridged [2]catenate **3**—The new DABCO-complexed catenate **3** was afforded through titration of **1** with DABCO in anisole. Formation of **3** could be easily followed by UV-Vis and steady-state fluorescence spectroscopies.^{61–67} The ZnP absorption in rotaxane **1** is observed at 428 (Soret band) and at 554/594 nm (Q-bands). Titration of rotaxane **1** with five-fold excess of DABCO causes a slight decrease in absorption and a bathochromic shift of 2 nm in the Soret band (Figure 3, left). Similar titration experiments with a zinc(II)tetr phenylporphyrin (ZnTPP) reference compound showed a shift of 5 nm in the Soret region (Figure 3, right), which is ascribed to the well-known 1:1 axial coordination of DABCO to ZnTPP.^{61–67} Further addition of DABCO (1×10^{-5} M) to the solution of ZnTPP reference causes a larger red shift (~ 10 nm) in Soret region (Figure 3, right), indicating coordination of two DABCO molecules to ZnTPP. Accordingly to these observations and in line with previous work,^{49,61–67} the slight redshift (2 nm) observed in the Soret band of rotaxane **1** is attributed to intramolecular coordination of a single DABCO guest between the two ZnP host moieties (as depicted in structure **3**, Figure 2). Complexation of two DABCO molecules to the rotaxane would result in larger redshifts (about 10 nm) in the Soret band, as observed in the ZnTPP control experiment.

The ZnP fluorescence of rotaxane **1** is significantly affected upon addition of DABCO (Figure 4, left). Bathocromic shifts of 10 and 7 nm are detected in **1** for the ZnP fluorescence maxima at 600 and 650 nm, respectively, and three isosbestic points are observed at 606, 636, and 663 nm, attesting to clean conversion of rotaxane **1** to the DABCO-bridged catenate **3**. Additional support for the rotaxane-to-catenane conversion is the gradual intensification (up to 20%) of the ZnP fluorescence in the titration experiments of **1**, which is in opposition to the reduction of the emission observed in the corresponding ZnTPP reference (Figure 4, right). We attribute this increase in emission intensity upon addition of DABCO to the unfolding of the rotaxane structure **1** to afford catenate **3**, in which the two ZnP groups are equidistant from the $[\text{Cu}(\text{phen})_2]^+$ complex as well as from the C₆₀ moiety.

1.3 - Copper-free rotaxane **4**—Cu-free rotaxanes and catenanes are usually afforded by treatment of their metalated analogs with KCN.⁶⁸ However, while it is possible to remove the Cu(I) template ion from rotaxane **1** using KCN, side reactions between nucleophilic CN[−] and the electrophilic fullerene cage result in addition of cyanide to C₆₀, as revealed by MALDI-TOF analysis.^{70,71} An obvious solution to this problem is to remove the Cu(I) template before introducing C₆₀ to the rotaxane structure. Accordingly, the synthetic route depicted in Scheme 1 was conceived. In this strategy, phen macrocycle **5**⁵⁵ (containing a peripheral benzaldehyde group for subsequent attachment of C₆₀ using a Prato reaction)⁷¹ was threaded by the phen-string like fragment **6** bearing terminal azide groups using classical Cu(I)-template conditions^{41–46} to afford pseudorotaxane **7**. ZnP groups were then appended to give rotaxane **8** using “click” chemistry,^{72,73} which was accomplished efficiently using techniques developed in our laboratory.^{53–57} The Cu(I) template ion was then removed from **8** using KCN,⁶⁸ yielding the Cu-free (ZnP)₂-rotaxane-benzaldehyde **9** in quantitative yield.

The ¹H NMR spectrum of Cu-free⁶⁸ rotaxane **9** (Figure 5, top) reveals the well-known^{3,41–46} downfield shift for the protons on the phenyl rings attached at the C-2 and C-9 positions of the phen moieties which are no longer entwined around the Cu(I) ion, attesting to successful demetalation. The presence of the aldehyde proton at 9.18 ppm shows that the peripheral formyl group did not undergo side reactions during the “click” stoppering process. The MALDI-TOF mass spectrum (Supporting Information, Figure S1) provided

structural confirmation, with an ion peak appearing at m/z 3482.82 ($M + H$)⁺ (calculated, 3481.65 for $C_{219}H_{232}N_{18}O_{15}Zn_2$).

A comparison between the 1H NMR spectra of macrocycle **5** and rotaxane **9** (see Figure 5) provides information about the structure of the system upon demetalation. After demetalation, the aromatic moieties belonging to the thread fragment appear in the usual region,^{41–46} while those on the macrocycle subunit are shifted upfield. In particular, the protons at C-5/6 and C-3/8 on the phen moiety (H_5 and H_3 , Figure 5) and the benzaldehyde group ($\underline{C}HO$, H_a and H_b) are shifted upfield by 2.2, 0.68, 0.66, and 0.26 ppm, respectively, suggesting that the phen moiety of the ring component is now in range of the strongly shielding ZnP ring current. According to the NMR data, it seems that the phen moiety on the ring component moves close to the ZnP groups upon demetalation, while the benzaldehyde moiety resides close to the phen moiety on the thread. Thus, we propose that the highly flexible Cu-free rotaxane adopts a conformation something like that shown for **9** in Scheme 1, driven principally by π - π interactions.

In the final step of the synthesis, C_{60} was introduced to rotaxane **9** by a Prato reaction using sarcosine,⁷¹ which proved to be problematic. Large excesses of C_{60} (15 eq) and sarcosine (20 eq) were needed to drive the reaction forward to **4**, which was isolated in only 6 % yield after 12 h of reflux in toluene and purification by preparative thin layer chromatography. Increasing the reaction time to 24 h led to even lower yields (2 %), while 36 h resulted in no product formation at all. Possibly, the excess C_{60} needed for formation of **4** promotes a retro-Prato reaction as the reaction time is extended, as previously reported.⁷⁴ The optimal reaction time was found to be 6 h, after which Cu-free rotaxane **4** was isolated in 13% yield after several chromatographic purification steps.

The MALDI-TOF spectrum of **4** (Figure 6) reveals a peak at m/z 4229⁷⁵ corresponding to $[M + H]^+$, along with a fragmentation pattern^{76–78} that is expected for a rotaxane structure^{41–46} with peripheral ZnP and C_{60} groups.^{58–59,69} The UV-Vis spectrum of **4** is essentially a linear combination of the UV-Vis absorption spectra of the C_{60} and ZnP moieties and corroborates the assigned structure (Figure 7). The characteristic absorption of the pyrrolidine- C_{60} moiety^{79,80} is observed at 327 nm, and the Soret and Q-bands of the ZnP group appear at 424, 554, and 594 nm, respectively.

The 1H NMR spectrum of rotaxane **4** is extremely complex, but suggests a supramolecular structure with the C_{60} well separated from the ZnP moieties, similar to that of **9**, indicating that even after addition of C_{60} , the phen moiety on the ring remains trapped between the two ZnP groups. Apparently, the strong phen-ZnP and ZnP-ZnP interactions preclude molecular reorganization that would bring the C_{60} moiety closer to the ZnP groups.^{81,82} On the basis of the photophysical properties of this material (vide infra), we propose that Cu-free rotaxane **4** adopts a structure similar to **9** (Scheme 1). This structure and conformation are consistent with the photophysical properties of this material (vide infra).

2 - Electrochemical Studies

These studies were carried out using *o*-dichlorobenzene (ODCB) as solvent in the presence of 0.1 M tetrabutylammonium perchlorate [$(n\text{-Bu})_4\text{NClO}_4$] as supporting electrolyte, using ferrocene/ferricenium as the internal reference. For **1**, the anodic scan reveals oxidations at +0.16 and +0.56 V (Supporting Information, Figure S2) corresponding to the coalescent first oxidations of $[\text{Cu}(\text{phen})_2]^+$ and ZnP and the second oxidation of ZnP, respectively. The very broad feature of the +0.16 V peak hampers an accurate determination/assignment of the individual oxidation potentials. Very similarly, in **2** the oxidations occur at +0.16 and +0.50 V.⁵⁹ In the cathodic scan, the reduction peak at –2.22 V **1** / –2.30 V **2** is assigned to the Cu^0/Cu^+ couple of $[\text{Cu}(\text{phen})_2]^+$, while those at –1.12, –1.50, –1.94, and –2.46 V relate to the

reduction of C₆₀ in **1** and **2**. In summary, no significant changes were observed in the oxidations and reductions in **1** and **2**, despite their dissimilar topology. Cu-free rotaxane **4** showed similar redox potentials to those of C₆₀ and ZnP model compounds, suggesting no significant interaction between the chromophores in the ground state, as already evidenced by UV-Vis analysis (*vide supra*).

3 - Photophysical Studies

3.1 - Reference and Model Compounds—Transient absorption studies of the reference and model compounds (Figure 8) were performed to facilitate interpretation of the photophysical dynamics of the more complex interlocked molecules. For C₆₀ reference compound **10**, femtosecond excitation at 387 nm led to transient absorption spectra with positive peaks at 510 and 910 nm, assigned to the singlet excited state of the C₆₀ which decays mainly by intersystem crossing to the low-lying triplet excited state.^{51,52} Exponential fits of the time profiles of these transient features gave a lifetime of 1.4 ns,^{51,52} similar to that of pristine C₆₀.^{79,80} In complementary flash photolysis experiments, transient absorption features for the triplet state, with maxima at 360 and 720 nm, were clearly detected. The long lifetime measured for this state, 20 μ s, was strongly quenched by purging the sample with O₂, confirming the triplet character of this transient species.

For the ZnP reference **11**, femtosecond excitation at 424 nm produced the characteristic transient features of ¹ZnP*, with positive absorption peaks at 460, 580, 625, and 720 nm and ground state bleaching at 420, 555, 600, and 685 nm. Deactivation of this state, occurring with a rate constant of 4×10^8 s⁻¹ ($\tau = 2.5$ ns), yielded the triplet excited state ³ZnP* with the long-lived ($\tau = 45$ μ s) transient absorption band at 840 nm.^{83,84}

Femtosecond transient absorption experiments of model [2]catenate **12** were carried out to investigate the interactions between the excited states of the [Cu(phen)₂]⁺ and C₆₀ moieties. Upon excitation of **12** at 387 nm, transient absorption spectra show maxima at 510 and 920 nm at early times (Figure S3, left), reflecting the rapid formation of the ¹C₆₀* state,^{51,52} which decays with accelerated dynamics (40 ps, see Figure S3, right) compared to model compound **10** (1.4 ns). This gives rise to a sharp transient peak at 1020 nm and a relatively broad band around 550 nm, which are assigned to the one-electron reduced form of the C₆₀ and the triplet excited [Cu(phen)₂]⁺ MLCT state, respectively.^{28,56} It can be concluded that the ¹C₆₀* is reductively quenched by the nearby [Cu(phen)₂]⁺ complex in **12** to produce the [Cu(phen)₂]^{2+–C₆₀•–} charge-separated state, while formation of the excited [Cu(phen)₂]⁺ MLCT state came from direct excitation of the complex at 387 nm. The transient features of the C₆₀•– species do not decay in the 3 ns time scale of our femtosecond experiments. Flash photolysis experiments with a 6 ns laser at 355 nm pulses were carried out and exponential analysis of the time profile at 1020 nm led to a lifetime of 15 ns, which is ascribed to charge recombination from the [Cu(phen)₂]^{2+–C₆₀•–} state, affording the ground state.

Finally, transient studies of rotaxane **8** (Scheme 1), lacking the C₆₀ moiety, were performed to assess the decay kinetics of the ZnP chromophore in the presence of the [Cu(phen)₂]⁺ moiety. After excitation of **8** at 424 nm in anisole, the transient absorption features of ¹ZnP* were detected (Figure 9, left), which decay biexponentially with lifetimes of 53 and 1360 ps (Figure 9, right). Each lifetime is assigned to the decay of one of the ZnP moieties, which appear to be independent of each other. Both lifetimes are considerably shorter than that of the ZnP reference compound **11** (2.4 ns), which suggests that an additional deactivation channel is active in **8**. Since there is no evidence for charge separation on this time scale, i.e., no absorption due to [Cu(phen)₂]²⁺ nor ZnP^{•+} was observed, a transduction of singlet excitation from photoexcited ZnP to [Cu(phen)₂]⁺ is proposed, as found previously with [2]catenate **2**.⁵⁹ Unfortunately, it was not possible to detect the transient absorption features

for the $[\text{Cu}(\text{phen})_2]^+$ excited state at 580 nm⁵⁶ since it is masked by the much stronger $^1\text{ZnP}^*$. In addition, $^3\text{ZnP}^*$ with transient absorption at 820 nm is clearly evident in the case of **8**, which suggests competition between the energy transfer and intersystem crossing processes.

3.2 - Rotaxane 1—Femtosecond excitation of rotaxane **1** at 424 nm in anisole or benzonitrile (PhCN) results in a transient spectrum dominated by the features of $^1\text{ZnP}^*$ (maxima at 460, 580, 625, 720 and 1020 nm as well as minima at 555, 600, and 680 nm, Figure 10). The time-absorption profiles reveal a much faster decay of $^1\text{ZnP}^*$ compared to that of the ZnP model **11**,⁸⁵ and very similar to the decay of the rotaxane **8** (Figure 9, right). The broad transient feature observed at 1020 nm at this time scale does not correspond to the fullerene radical anion $\text{C}_{60}^{\bullet-}$, but to the excited state of the $[\text{Cu}(\text{phen})_2]^+$ complex.⁵⁷ Therefore, no hints of an electron transfer process, i.e., transient features of $[\text{Cu}(\text{phen})_2]^{2+}$, ZnP^{*+} or $\text{C}_{60}^{\bullet-}$, were detected. This proves that the rapid deactivation of $^1\text{ZnP}^*$ in rotaxane **1** occurs by the same process as in rotaxane **8**, involving only the $[\text{Cu}(\text{phen})_2]^+$ complex and not C_{60} . Thus, singlet-singlet energy transfer (EnT) from $^1\text{ZnP}^*$ to the $[\text{Cu}(\text{phen})_2]^+$ is proposed, in competition with intersystem crossing to generate $^3\text{ZnP}^*$.

Biexponential functions were needed to accomplish an accurate multiwavelength analysis of the data. For the decay of $^1\text{ZnP}^*$ in **1** lifetimes of 61 and 400 ps were obtained in anisole (Figure 9, right), each lifetime corresponding to one of the ZnP moieties. The flexibility of the linker connecting the ZnP and the $[\text{Cu}(\text{phen})_2]^+$ moieties in rotaxane **1** allows molecular conformations in which the ZnP moieties are at different distances relative to the $[\text{Cu}(\text{phen})_2]^+$ complex. The distance between the ZnP and $[\text{Cu}(\text{phen})_2]^+$ moieties clearly plays a major role in the energy transfer kinetics. These findings convincingly support the previously proposed folded structure for rotaxane **1** based on ^1H NMR analysis and computational calculation.⁵⁸

Femtosecond excitation of rotaxane **1** in anisole or PhCN at 387 nm leads to the immediate formation of $^1\text{ZnP}^*$ and $^1\text{C}_{60}^*$. While the former has already been described, we identified the latter as a weak transient with an absorption maximum around 900 nm (Figure S4, left). Lifetimes of 75 and 212 ps in PhCN and anisole, respectively, were obtained by fitting the decay profiles at 900 nm, in sharp contrast to the 1.4 ns $^1\text{C}_{60}^*$ lifetime measured for C_{60} model compound **10**. Simultaneously with the decay of the transient at 900 nm^{51,52}, a new signal develops in the near infrared region, with a maximum at 1020 nm, which is the signature of $\text{C}_{60}^{\bullet-}$.^{79,80} The formation of $\text{C}_{60}^{\bullet-}$, which is stable on the femto- and picosecond time scales, is attributed to charge separation from the activated $[\text{Cu}(\text{phen})_2]^+$ complex or $^1\text{C}_{60}^*$ to yield $(\text{ZnP})_2\text{--}[\text{Cu}(\text{phen})_2]^{2+}\text{--}\text{C}_{60}^{\bullet-}$. Unfortunately, the characteristic transient absorption of the $[\text{Cu}(\text{phen})_2]^{2+}$ species⁵⁶ is masked by that of $^1\text{ZnP}^*$, which is also formed upon excitation at 387 nm.

In the nanosecond time regime, upon excitation of **1** at 355 nm, the differential absorption spectrum is dominated in the visible region by ZnP^{*+} , centered at 660 nm, and by a maximum at 1020 nm in the near infrared corresponding to $\text{C}_{60}^{\bullet-}$ (Figure 11, top). The best fit for the decay of $\text{C}_{60}^{\bullet-}$ in the near infrared involves a biexponential function, with the short-lived component having values of 54 ns in anisole and 18 ns in PhCN (Figure 11, middle). The latter value resembles quite well that of the model compound **12** (15 ns in PhCN), and is therefore attributed to decay of the $[\text{Cu}(\text{phen})_2]^{2+}\text{--}\text{C}_{60}^{\bullet-}$ radical ion pair state, which undergoes charge recombination to give the ground state. The long-lived component at 1020 nm has a lifetime of 234 ns in anisole, which matches the decay kinetics (240 ns) of ZnP^{*+} at 660 nm (Figure 11, bottom) in the same solvent. This excellent agreement suggests that the process responsible for both decays is charge recombination in the $(\text{ZnP})_2^{\bullet+-}\text{--}[\text{Cu}(\text{phen})_2]^+\text{--}\text{C}_{60}^{\bullet-}$ charge separated radical pair (CSRP) state. In addition, a long-lived

component ($2.8\text{ }\mu\text{s}$) in the decay extending from 660 nm to 740 nm is assigned to the triplet excited state of C_{60} , which is confirmed by diffusion-controlled oxygen quenching in O_2^- -saturated solutions.

The most likely route for formation of $\text{ZnP}^{\bullet+}$ is charge shift from the photo-oxidized $[\text{Cu}(\text{phen})_2]^{2+}$ complex to ZnP , which yields the $(\text{ZnP})_2^{\bullet+}-[\text{Cu}(\text{phen})_2]^+-\text{C}_{60}^{\bullet-}$ long distance charge separated state. This charge shift process competes with charge recombination in $(\text{ZnP})_2-[\text{Cu}(\text{phen})_2]^{2+}-\text{C}_{60}^{\bullet-}$ and occurs in the nanosecond time domain, as previously found for the related catenane **2**⁵⁹. An alternative source of $\text{ZnP}^{\bullet+}$ could involve the formation of $(\text{ZnP})_2^{\bullet+}-[\text{Cu}(\text{phen})_2]-\text{C}_{60}^{\bullet-}$ charge separated state, containing oxidized ZnP and reduced $[\text{Cu}(\text{phen})_2]$ moieties, but an estimate of the energy level of this state based on the electrochemical potentials of ZnP^+ ($+0.16\text{ V}$) and $[\text{Cu}(\text{phen})_2]$ (-2.22 V) is 2.38 eV , which is energetically prohibitive.

In summary, photoinduced charge separation in **1** followed by a charge shift transforms the initially formed $(\text{ZnP})_2-[\text{Cu}(\text{phen})_2]^{2+}-\text{C}_{60}^{\bullet-}$ CS state into the long-distance $\text{ZnP}^{\bullet+}-[\text{Cu}(\text{phen})_2]^+-\text{C}_{60}^{\bullet-}$ CSRP state. Based on the electrochemical data, these two states are close in energy. However, the photophysical data strongly suggest that there is an appreciable driving force which powers the charge shift, so that the two states cannot be in equilibrium, i.e., charge recombination in the initially formed CS state competes with a charge shift process to give the long-distance CSRP state. The slower charge recombination rate in the long-distance CSRP state compared with that in the tighter CS state is attributed to the much longer distance between the oxidized $(\text{ZnP})_2^{\bullet+}$ and reduced $\text{C}_{60}^{\bullet-}$ moieties. The aforementioned findings, together with the electrochemical data, allow the construction of the energy diagram shown in Figure 12, which illustrates the photophysical decay pathway in PhCN for rotaxane **1** upon electronic excitation in the ZnP Soret band.

3.3 - DABCO-complexed-catenate 3—Femto- and nanosecond absorption spectroscopy in anisole using 424 nm , 387 nm , or 355 nm excitation was used to assess the effect of the DABCO-induced rotaxane-to-catenane conversion of **1** to **3** on the ET dynamics. The concentration of **1** was kept constant ($5 \times 10^{-6}\text{ M}$), while the DABCO concentration was gradually increased up to $2.5 \times 10^{-5}\text{ M}$. At the highest DABCO concentration, upon excitation at 424 nm , the transient absorption changes are virtually identical to those observed for the noncomplexed rotaxane **1** (compare Figures 10 and 13). The visible region is dominated by the transient feature of ${}^1\text{ZnP}^*$ with maxima at 465 , 585 , 630 , and 710 nm and minima at 565 , 605 , and 680 nm (Figure 13, left). Upon comparison of the time profiles at 460 nm for **1** and **3** (Figure 13, right), an important difference is observed. Unlike the biexponential function needed to obtain an accurate fit of the data in the case of **1**, a monoexponential function with a lifetime of 220 ps was sufficient for **3**.⁸⁶ Assuming that the same sequence of EnT and ET processes occur in the case of **3** as depicted in Figure 12, a single decay lifetime indicates identical kinetic behavior of the two ZnP moieties. Thus, DABCO coordination forces both ZnP s to be equidistant with respect to $[\text{Cu}(\text{phen})_2]^+$, resulting in identical ET kinetics for the two ZnP s.

On the other hand, femtosecond excitation of **3** at 387 nm in anisole induces the rapid formation of ${}^1\text{C}_{60}^*$, although the strong transient signal of ${}^3\text{ZnP}^*$ at 840 nm hampers the clear identification of the ${}^1\text{C}_{60}^*$ transient band at 920 nm . As in the case of **1**, this signal decays with accelerated dynamics, $\tau = 260\text{ ps}$, (Figure 14, left) compared to the C_{60} reference **10** (1.4 ns). In parallel to this decay, the $\text{C}_{60}^{\bullet-}$ band is detected at 1020 nm which indicates that ET is responsible for the rapid deactivation of ${}^1\text{C}_{60}^*$ (Figure 14, right). Since the distance to ZnP is rather long and the $\text{ZnP}^{\bullet+}$ transient band at 660 nm is absent, the ET must originate in the $[\text{Cu}(\text{phen})_2]^+$ complex, as previously described for rotaxane **1** and model [2]catenate **12**. Turning to the decay at 920 nm , the lifetime of 260 ps , which is very

similar to that measured for **1** in anisole (212 ps), testifies to no significant change in the ET dynamics between **1** and **3**. This outcome is not unexpected, since DABCO complexation affects only the ZnP-[Cu(phen)₂]⁺ distance.

Turning to the nanosecond flash photolysis experiments, the signature of ZnP^{•+} dominates the visible region upon excitation of **3** at 355 nm in anisole, while transient absorption in the near-infrared region again indicates the formation of C₆₀^{•-} (Figure 15, left). This is in line with those transient spectra seen for rotaxane **1** (Figure 11, top) and confirms the formation of the ZnP^{•+}-[Cu(phen)₂]⁺-C₆₀^{•-} CSRP state upon excitation of the DABCO-catenate **3**. The decay of the C₆₀^{•-} anion at 1020 nm (Figure 15, right) obeys a biexponential function, with components of 54 ns and 1.03 μs. As in the case of rotaxane **1**, the short- and long-lived components can be assigned to charge recombination of the ZnP-[Cu(phen)₂]²⁺-C₆₀^{•-} (CS) and ZnP^{•+}-[Cu(phen)₂]⁺-C₆₀^{•-} (CSRP) states. The kinetic trace at 660 nm, corresponding to the decay of the ZnP^{•+} cation, requires a mono-exponential function fitting that yields a lifetime of 1.3 μs, which is fairly close to that of the long-lived component (1.03 μs) at 1020 nm. Therefore, the long-lived component at 1020 nm can be safely attributed to charge recombination from the ZnP^{•+}-[Cu(phen)₂]⁺-C₆₀^{•-} CSRP state. Thus, complexation of rotaxane **1** with DABCO to give a catenated molecule does not affect the photophysical pathway taken upon excitation at 355 nm.

On one hand, it is clear that DABCO complexation has virtually no impact on the decay kinetics of the tight (ZnP)₂-[Cu(phen)₂]²⁺-C₆₀^{•-} CS state, since the charge recombination rates measured at 1020 nm are exactly the same (54 ns in anisole) for rotaxane **1** and DABCO-bridged [2]catenate **3**. On the other hand, the kinetics associated with charge recombination in the long-distance (ZnP)₂^{•+}-[Cu(phen)₂]⁺-C₆₀^{•-} CSRP state are quite different (Figure 15, right): for DABCO-bridged [2]catenate **3** the CSRP lifetime of 1.03 μs in anisole is more than four times that of rotaxane **1** (0.24 μs in anisole). Indeed, the lifetime of the CSRP state in **3** approaches the lifetimes of 1.1 μs (PhCN) and 1.5 μs (THF) determined for the deactivation of the same CSRP state in [2]catenate **2**,⁵⁹ consistent with the topological similarity of [2]catenate **2** and the DABCO-bridged [2]catenate **3**.

Cu-free rotaxane 4: In stark contrast to rotaxane **1**, steady-state fluorescence experiments revealed the lack of appreciable ¹ZnP* fluorescence quenching in **4** (Figure 16, left), suggesting that the ZnP_s in **4** are not close to C₆₀, preventing direct electronic interaction between the chromophores. In line with the fluorescence experiments, transient absorption studies (Figure 16, right) revealed only signals corresponding to the formation of ZnP^{83,84} and C₆₀^{51,52} triplet excited states. Upon photoexcitation of **4** at 355, 387 or 420 nm in solvents of different polarity, ranging from anisole to dimethylformamide with dielectric constants as high as 36.8, no evidence for ET was obtained. It seems that the interactions between the ZnP_s as well as those between the ZnP and the free-phen chelates are strong enough to prevent close approach^{81,82} of the C₆₀ subunit in **4**. These surprising results highlight the critical importance of the central [Cu(phen)₂]⁺ complex in the photophysics of rotaxane **1** as well as [2]catenates **2** and **3**. The [Cu(phen)₂]⁺ complex provides the structural organization together with electronic properties needed to mediate ET reactions between the distant ZnP and C₆₀ groups in our interlocked architectures.

5. Comparison between rotaxane and catenane structures

An attempt to reach general conclusions about the different photophysical properties of our complex rotaxanes and catenanes is difficult because of the many parameters involved in the light induced processes. However, the data presented here and in our previous manuscript⁵⁹ permit us to draw some conclusions in order to gain insight into the connection between molecular topology and ET dynamics in these systems.

Our investigation reveals that catenanes and rotaxanes assembled through a central $[\text{Cu}(\text{phen})_2]^+$ complex and bearing appended ZnP and C_{60} groups present a common photophysical pathway decay. In all systems, excitation of the ZnP unit at 420 nm yields $^1\text{ZnP}^*$, which is rapidly quenched through energy transfer (EnT) to the $[\text{Cu}(\text{phen})_2]^+$ complex. The MLCT state thereby produced decays through ET to the fullerene, generating the intermediate $\text{ZnP}-[\text{Cu}(\text{phen})_2]^{2+}-\text{C}_{60}^{\bullet-}$ CS state, featuring an oxidized copper complex and a reduced fullerene. A subsequent charge shift from the oxidized copper complex to ZnP yields the final long-distance $\text{ZnP}^{\bullet+}-[\text{Cu}(\text{phen})_2]^+-\text{C}_{60}^{\bullet-}$ CSRP state, where the positive charge is located on ZnP and the electron is on C_{60} .

From electrochemical investigations, we have found that the photoinduced CS states formed in both rotaxane **1** and catenate **2** are virtually isoenergetic despite their distinct topologies. The topological and conformational differences between rotaxane and catenane structures do not significantly affect electronic interactions in the ground state. Therefore, the dissimilar photophysical dynamics observed in our interlocked systems cannot be explained on a thermodynamic basis. Instead, we consider the kinetics parameters related to the decays of the excited and charge separated states in these systems, where the distinct rotaxane and catenane topological features can be considered.

Transient absorption experiments clearly show a biexponential decay for the $^1\text{ZnP}^*$ in rotaxane **1** with components of 61 ps and 400 ps, revealing that the two ZnP “stoppering” groups are not equivalent. On the other hand, a monoexponential fit with a component of 500 ps is sufficient to satisfy the decay of the $^1\text{ZnP}^*$ in catenate **2**,⁵⁹ where the chromophores are as far as possible from each other. Since the kinetics of EnT and ET transfer processes are extremely dependent upon the distance between the chromophores, we conclude that rotaxane **1** adopts the proposed folded molecular conformation with the ZnP groups at different distances from the $[\text{Cu}(\text{phen})_2]^+$ complex and the C_{60} .

Interestingly, the same analysis shows that the ZnPs in model rotaxane **8**, which lacks the C_{60} moiety, also presents biexponential decay for $^1\text{ZnP}^*$, indicating a folded conformation for this rotaxane as well. However, a closer inspection of the $^1\text{ZnP}^*$ lifetimes determined for **1** and **8** reveals that introduction of the bulky carbon cage into the ring component of the rotaxane structure affects the long component of the $^1\text{ZnP}^*$ decay (400 ps for **1** and 1360 ps for **8**), whereas it has virtually no effect on the short component (61 ps in **1** and 53 ps in **8**). We suggest that attachment of C_{60} to the rotaxane architecture brings the previously distant ZnP group closer to the $[\text{Cu}(\text{phen})_2]^+$ complex, resulting in a more compact distribution of the ZnPs in **1** than in **8**. We also believe that these intramolecular interactions between the ZnPs and $[\text{Cu}(\text{phen})_2]^+$ complex affect the rate of ET from the $[\text{Cu}(\text{phen})_2]^+$ complex to $^1\text{C}_{60}^*$, as revealed by the longer lifetime observed for the $^1\text{C}_{60}^*$ moiety in rotaxane **1** (75 ps) compared to that in catenate **2** (33 ps), which lacks such interactions.

A slightly longer lifetime for the neighbouring $\text{ZnP}-[\text{Cu}(\text{phen})_2]^{2+}-\text{C}_{60}^{\bullet-}$ state generated through ET from the $[\text{Cu}(\text{phen})_2]^+$ complex to C_{60} is observed in rotaxane **1** (18 ns) when compared to catenate **2** (15 ns). This neighbouring radical ion pair state is characterized by an oxidized copper complex and a reduced fullerene. The formation of this state is accompanied by a change in the formal oxidation state of the copper ion from +1 to +2. There is an extensive body of literature illustrating that oxidation of the Cu(I) to Cu(II) metal center in $[\text{Cu}(\text{phen})_2]^+$ complexes causes a flattening of the original tetrahedral spatial arrangement of the phen ligands in order to facilitate coordination of a fifth ligand to the Cu(II) ion, which prefers a pentacoordinate environment.^{87,88} This structural rearrangement of the inner coordination sphere is known to have important consequences on the excited states of $[\text{Cu}(\text{phen})_2]$ complexes.

In our case, we believe the flattening caused upon photo-oxidation of the $[\text{Cu}(\text{phen})_2]^+$ complex should improve the $\pi\text{-}\pi$ interactions between the phen ligands and the nearby ZnP_s in the compact structure of rotaxane **1**, which might help to stabilize the photo-generated $[\text{Cu}(\text{phen})_2]^{2+}$ complex, resulting in a longer lifetime for the $(\text{ZnP})_2\text{-}[\text{Cu}(\text{phen})_2]^{2+}\text{-C}_60^{\bullet-}$ tight CS state. In the case of catenate **2**, the flattening process also takes place upon oxidation of the $[\text{Cu}(\text{phen})_2]^+$ complex, but has comparatively little effect on the intramolecular interactions between the chromophores because they are so far apart in this rigid structure.

The most significant effect of the distinct rotaxane and catenane topologies on the ET dynamics of our systems can be contemplated by comparing the charge recombination rate of the various long-distance $\text{ZnP}^{\bullet+}\text{-}[\text{Cu}(\text{phen})_2]^+\text{-C}_60^{\bullet-}$ CSRP states. Thus, the CSRP lifetime in catenate **2** is 1.1 μs in PhCN, about four times as long as that in rotaxane **1** (0.24 μs) under the same conditions. We ascribe this difference to the rigidity of the catenane structure, which keeps the chromophores far apart, spatially isolating the radical ions, which in turn reduces the charge recombination rate.

This topological effect is most dramatically demonstrated by the investigation of the photophysical properties of the DABCO-bridged catenate **3**. Complexation of a single DABCO molecule guest in between the two ZnP_s of **1** promotes a rotaxane to catenane conversion and significantly increases the rigidity of the system. Accordingly, the lifetime of the long-distance $\text{ZnP}^{\bullet+}\text{-}[\text{Cu}(\text{phen})_2]^+\text{-C}_60^{\bullet-}$ state is more than four times longer in **3** (1.03 μs) than in **1** (0.24 μs) and approaches that in catenate **2** (1.1 μs in PhCN and 1.5 μs in THF). These findings unambiguously reveal that adoption of a rigid catenane topology from a conformational much more flexible rotaxane inhibits the charge recombination process.

Conclusions

The recent synthetic techniques developed in our group have allowed the preparation of $[\text{Cu}(\text{phen})_2]^+$ -based rotaxane and catenane architectures possessing ZnP and C₆₀ subunits linked by identical connecting groups, rendering these structures ideal models for investigation of topological effects on electron transfer dynamics. The choice of a central photoactive $[\text{Cu}(\text{phen})_2]^+$ complex as template to assemble the interlocked systems proved to be crucial. The metallic core turned out to be essential for a good long distance electronic communication between ZnP and C₆₀, as removing the Cu(I) template ion completely shut down the ET processes. The introduction of C₆₀ as the ultimate electron acceptor into $[\text{Cu}(\text{phen})_2]^+$ based rotaxanes and catenanes was also crucial. The outstanding redox and spectroscopic properties of C₆₀ permitted the characterization of all intermediates involved in the photoinduced processes of these interlocked systems. Thus, our investigation yielded a useful set of thermodynamic and kinetic parameters not previously available, which allowed a critical comparison to be made between the photophysical properties of rotaxanes and catenanes, providing new insight into topological and conformational effects on electron transfer dynamics in extended artificial photosynthetic model systems.

Supplementary Material

Refer to Web version on PubMed Central for supplementary material.

Acknowledgments

Support of the work at NYU by a grant from the National Science Foundation (CHE-0647334) is acknowledged with grateful appreciation. This investigation was conducted in part using an instrumental facility at NYU constructed with support from Research Facilities Improvement Grant Number C06 RR-16572-01 from the National Center for Research Resources, National Institutes of Health. We also would like to thank the Deutsche

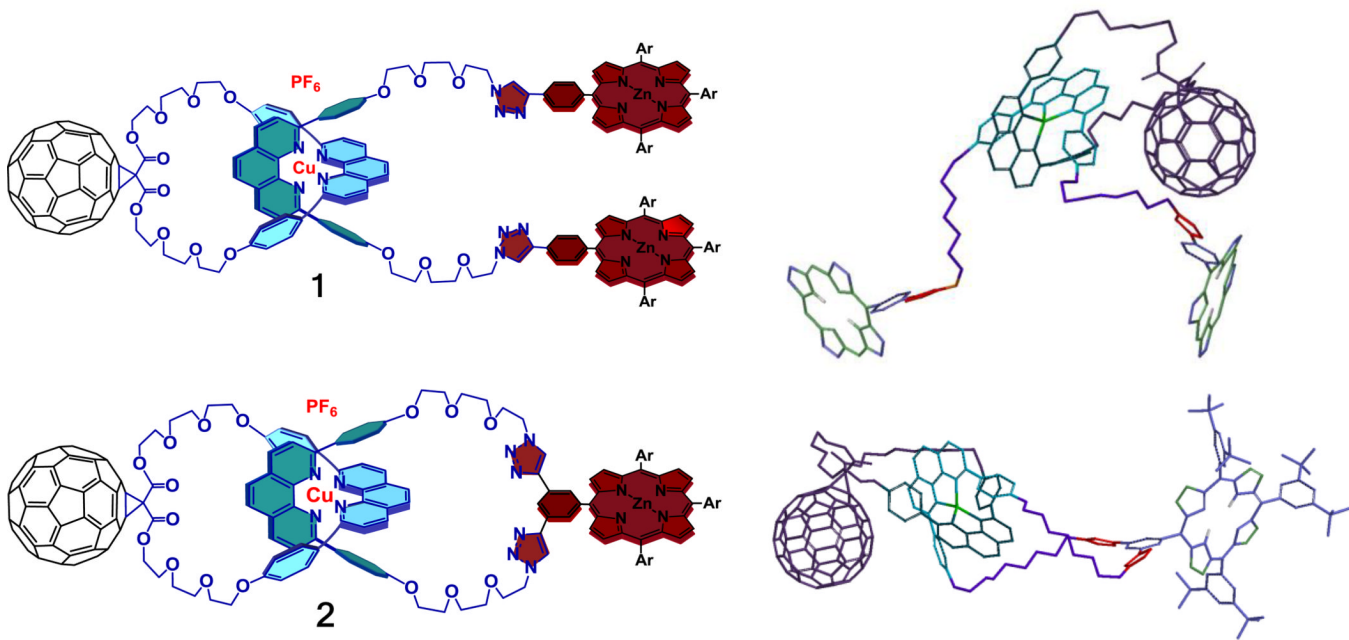
Forschungsgemeinschaft (SFB 583), FCI and Office of Basic Energy Sciences of the U.S. Department of Energy for financial support.

References

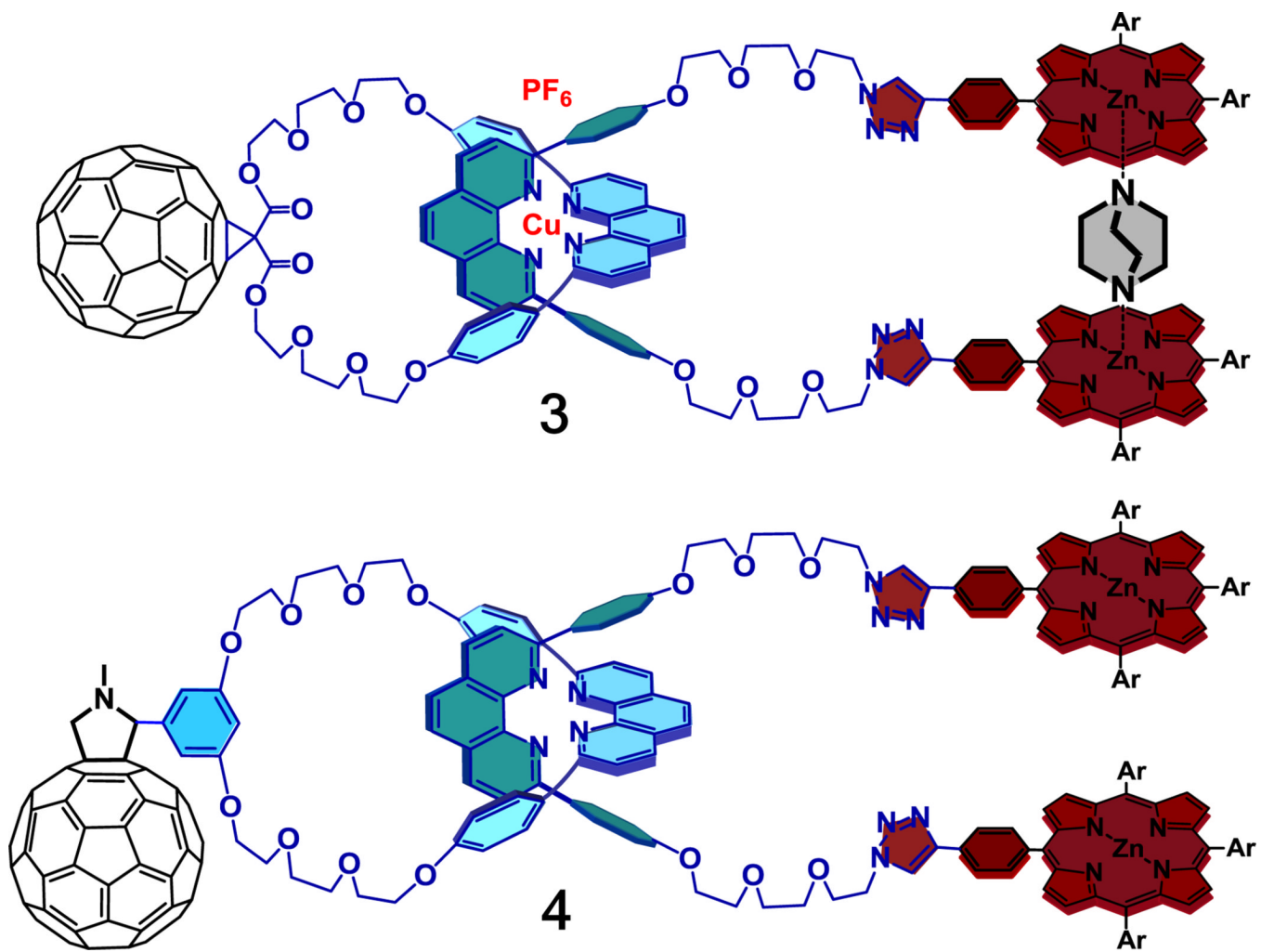
1. Sauvage J-P. *Acc. Chem Res.* 1990; 23:319.
2. Amabilino DB, Stoddart JF. *Chem. Rev.* 1995; 95:2725.
3. Sauvage, J-P.; Dietrich-Buchecker, CO. *Molecular Catenanes, Rotaxanes and Knots*. Weinheim: Wiley-VCH; 1999.
4. Balzani V, Credi A, Raymo FM, Stoddart JF. *Angew. Chem. Int. Ed.* 2000; 39:3348.
5. Crowley JD, Goldup SM, Lee A, Leigh DA, McBurney RT. *Chem. Soc. Rev.* 2009; 38:1530. [PubMed: 19587949]
6. Beves JE, Blight BA, Campbell CJ, Leigh DA, McBurney RT. *Angew. Chem. Int. Ed.* 2011; 50:9260.
7. Wang X, Bao X, McFarland-Mancini M, Isaacsohn I, Drew AF, Smithrud DB. *J. Am. Chem. Soc.* 2007; 129:7284. [PubMed: 17516642]
8. Coti KK, Belowich ME, Liong M, Ambrogio MW, Lau YA, Khatib HA, Zink JI, Khashab NM, Stoddart JF. *Nanoscale.* 2009; 1:16. [PubMed: 20644858]
9. Fernandes A, Viterisi A, Coutrot F, Potok S, Leigh DA, Aucagne V, Papot SA. *Angew. Chem. Int. Ed.* 2009; 48:6443.
10. Thordarson P, Bijsterveld JA, Rowan AE, Nolte RJM. *Nature.* 2003; 424:915. [PubMed: 12931181]
11. Crowley JD, Goldup SM, Gowans ND, Leigh DA, Ronaldson VE, Slawin AMZ. *J. Am. Chem. Soc.* 2010; 132:6243. [PubMed: 20377187]
12. Crowley JD, Hanni KD, Leigh DA, Slawin AMZ. *J. Am. Chem. Soc.* 2010; 132:5309. [PubMed: 20334379]
13. Harada A, Hashidzume A, Yamaguchi H, Takashima Y. *Chem. Rev.* 2009; 109:5974. [PubMed: 19736930]
14. Olson MA, Braunschweig AB, Fang L, Ikeda T, Klajn R, Trabolsi A, Wesson PJ, Benitez D, Mirkin CA, Grzybowski BA, Stoddart JF. *Angew. Chem. Int. Ed.* 2009; 48:1792.
15. Kuang X, Wu X, Donahue JP, Huang J, Lu CZ. *Nature Chem.* 2010; 2:461. [PubMed: 20489714]
16. Collin JP, Frey J, Heitz V, Sauvage J-P, Tock C, Allouche L. *J. Am. Chem. Soc.* 2009; 131:5609. [PubMed: 19334735]
17. Sato Y, Yamasaki R, Saito S. *Angew. Chem. Int. Ed.* 2009; 48:504.
18. Langton MJ, Matichak JD, Thompson AL, Anderson HL. *Chem. Sci.* 2011; 2:1897.
19. Balzani V, Clemente-Leon M, Credi A, Ferrer B, Venturi M, Flood AH, Stoddart JF. *Proc. Natl. Acad. Sci. USA.* 2006; 103:1178. [PubMed: 16432207]
20. Balzani V, Credi A, Venturi M. *Chem. Soc. Rev.* 2009; 38:1542. [PubMed: 19587950]
21. Sauvage J-P, Collin J-P, Durot S, Frey J, Heitz V, Sour A, Tock C. *C. R. Chimie.* 2010; 13:315.
22. Balzani, V.; Credi, A.; Venturi, M. *Molecular Devices and Machines-A Journey into the Nano World*. Weinheim: Wiley-VCH; 2003.
23. Li H, Fahrenbach AC, Coskun A, Zhu Z, Barin G, Zhao Y-L, Botros YY, Sauvage J-P, Stoddart JF. *Angew. Chem. Int. Ed.* 2011; 50:6782.
24. Zhang H, Kou X-X, Zhang Q, Qu D-H, Tian H. *Org. Biomol. Chem.* 2011; 9:4051. [PubMed: 21505698]
25. Jakob M, Berg A, Levanon H, Schuster DI, Megiatto JD Jr. *J. Phys. Chem. A.* 2011; 115:5044. [PubMed: 21528881]
26. Duo Y, Jacob S, Abraham W. *Org. Biomol. Chem.* 2011; 9:3549. [PubMed: 21445383]
27. Benniston AC, Harriman A, Lynch VM. *J. Am. Chem. Soc.* 1995; 117:5275.
28. Armaroli N, Diederich F, Dietrich-Buchecker CO, Flamigni L, Marconi G, Nierengarten J-F, Sauvage J-P. *Chem. Eur. J.* 1998; 4:406.

29. Linke M, Chambron J-C, Heitz V, Sauvage J-P, Encinas S, Barigelletti F, Flamigni L. *J. Am. Chem. Soc.* 2000; 122:11834.
30. Armaroli N. *Chem. Soc. Rev.* 2001; 30:113.
31. Da Ros T, Guldi DM, Morales AF, Leigh DA, Prato M, Turco R. *Org. Lett.* 2003; 5:689. [PubMed: 12605491]
32. Watanabe N, Kihara N, Furusho Y, Takata T, Araki Y, Ito O. *Angew. Chem. Int. Ed.* 2003; 42:681.
33. Sandanayaka ASD, Ito O. *J. Porph. Phthal.* 2009; 13:1017.
34. D'Souza F, Subbaiyan NK, Xie Y, Hill JP, Ariga K, Ohkubo K, Fukuzumi S. *J. Am. Chem. Soc.* 2009; 131:16138. [PubMed: 19886697]
35. Sandanayaka ASD, Sasabe H, Takata T, Ito O. *J. Photochem. Photobiol. C: Photochem. Rev.* 2011; 11:73.
36. Balzani V, Credi A, Langford SJ, Prodi A, Stoddart JF, Venturi M. *Supramol. Chem.* 2001; 13:303.
37. Linke M, Fujita N, Chambron JC, Heitz V, Sauvage J-P. *New J. Chem.* 2001; 25:790.
38. Nakamura Y, Minami S, Lizuka K, Nishimura J. *Angew. Chem. Int. Ed.* 2003; 42:3158.
39. Au-Yeung HY, Cougnon FBL, Otto S, Pantos GD, Sanders JKM. *Chem. Sci.* 2010; 1:567.
40. Cao D, Amelia M, Klivansky LM, Koshkakaryan G, Khan SI, Semeraro M, Silvi S, Venturi M, Credi A, Liu Y. *J. Am. Chem. Soc.* 2010; 132:1110. [PubMed: 20043674]
41. Chambron J-C, Harriman A, Heitz V, Sauvage J-P. *J. Am. Chem. Soc.* 1993; 115:7419.
42. Solladie N, Chambron J-C, Sauvage J-P. *J. Am. Chem. Soc.* 1999; 121:3684.
43. Andersson M, Linke M, Chambron J-C, Davidsson J, Heitz V, Hammarström L, Sauvage J-P. *J. Am. Chem. Soc.* 2000; 122:3526.
44. Andersson M, Linke M, Chambron J-C, Davidsson J, Heitz V, Hammarström L, Sauvage J-P. *J. Am. Chem. Soc.* 2002; 124:4347. [PubMed: 11960464]
45. Flamigni L, Talarico AM, Chambron J-C, Heitz V, Linke M, Fujita N, Sauvage J-P. *Chem. Eur. J.* 2004; 10:2689. [PubMed: 15195300]
46. Flamigni L, Heitz V, Sauvage J-P. *Struc. Bond.* 2006; 121:217.
47. Li K, Bracher PJ, Guldi DM, Herranz MA, Echegoyen L, Schuster DI. *J. Am. Chem. Soc.* 2004; 126:9156. [PubMed: 15281785]
48. Li K, Schuster DI, Guldi DM, Herranz MA, Echegoyen L. *J. Am. Chem. Soc.* 2004; 126:3388. [PubMed: 15025442]
49. Schuster DI, Li K, Guldi DM, Ramey J. *Org. Lett.* 2004; 6:1919. [PubMed: 15176783]
50. Schuster DI, Li K, Guldi DM. *C. R. Chimie.* 2006; 9:892.
51. Guldi DM. *Chem. Commun.* 2000:321.
52. Guldi DM, Prato M. *Acc. Chem. Res.* 2000; 33:695. [PubMed: 11041834]
53. Megiatto JD Jr, Schuster DI. *J. Am. Chem. Soc.* 2008; 130:12872. [PubMed: 18767850]
54. Megiatto JD Jr, Schuster DI. *Chem. Eur. J.* 2009; 15:5444. [PubMed: 19360832]
55. Megiatto JD Jr, Schuster DI. *New J. Chem.* 2010; 34:276.
56. Megiatto JD Jr, Schuster DI, Palkar A, Herranz MA, Echegoyen L, Abwandner S, de Miguel G, Guldi DM. *J. Phys. Chem. B.* 2010; 114:14408. [PubMed: 20518479]
57. Megiatto JD Jr, Spencer R, Schuster DI. *J. Mater. Chem.* 2011; 21:1544.
58. Megiatto JD Jr, Spencer R, Schuster DI. *Org. Lett.* 2009; 11:4152. [PubMed: 19685862]
59. Megiatto JD Jr, Schuster DI, Abwandner S, De Miguel G, Guldi DM. *J. Am. Chem. Soc.* 2010; 132:3847. [PubMed: 20196597]
60. Sauvage proposed the names catenate for interlocked systems bearing a transition metal complex template (also called metallo-catenanes) and catenand for the corresponding metal-free structure.
61. Hunter CA, Meah MN, Sanders JKM. *J. Am. Chem. Soc.* 1990; 112:5773.
62. Fujisawa J, Ishii K, Ohba Y, Yamauchi S. *J. Phys. Chem. A.* 1997; 101:5869.

63. D'Souza F, Deviprasad GR, Rahman MS, Choi JP. Inorg. Chem. 1999; 38:2157. [PubMed: 11671000]
64. Armaroli N, Diederich F, Echegoyen L, Habicher T, Flamigni L, Marconi G, Nierengarten J-F. New J. Chem. 1999;77.
65. Da Ros T, Prato M, Guldi DM, Ruzzi M, Pasimeni L. Chem. Eur. J. 2001; 7:816. [PubMed: 11288873]
66. Guldi DM, Luo C, Swartz A, Scheloske M, Hirsch A. Chem. Comm. 2001; 12:1066.
67. Baldini L, Ballester P, Casnati A, Gomila RM, Hunter CA, Sansone F, Ungaro R. J. Am. Chem. Soc. 2003; 125:14181. [PubMed: 14611257]
68. Albrecht-Gary AM, Saad Z, Dietrich-Buchecker CO, Sauvage J-P. J. Am. Chem. Soc. 1985; 107:3205.
69. Megiatto JD Jr, Schuster DI. Org. Lett. 2011; 13:1808. [PubMed: 21384822]
70. Hirsch, A.; Brettreich, M. *Fullerenes*. Weinheim: Wiley-VCH; 2005.
71. Maggini M, Scorrano G, Prato M. J. Am. Chem. Soc. 1993; 115:9798.
72. Kolb HC, Finn MG, Sharpless KB. Angew. Chem. Int. Ed. Engl. 2001; 40:2004. [PubMed: 11433435]
73. Tornøe C, Christensen C, Meldal M. J. Org. Chem. 2002; 67:3057. [PubMed: 11975567]
74. Lukyanova O, Cardona CM, Altable M, Filippone S, Domenech AM, Martín N, Echegoyen L. Angew. Chem. Int. Ed. 2006; 45:110.
75. This material requires *m/z* 4228. 19, calculated for C₂₈₁H₂₃₇N₁₉O₁₄Zn₂
76. Vetter W, Schill G. Tetrahedron. 1967; 23:3079.
77. Bitsch F, Dietrich-Buchecker CO, Khemiss AK, Sauvage J-P, Dorsselaer AV. J. Am. Chem. Soc. 1991; 113:4023.
78. Mohr B, Sauvage J-P, Grubbs RH, Weck M. Angew. Chem. Int. Ed. 1997; 36:1308.
79. Gust D, Moore TA, Moore AL. Acc. Chem. Res. 1993; 26:198.
80. Guldi DM, Zerbetto F, Georgakilas V, Prato M. Acc. Chem. Res. 2005; 38:38. [PubMed: 15654735]
81. Olmstead MM, Costa DA, Maitra K, Noll BC, Phillips SL, Van Calcar PM, Balch AL. J. Am. Chem. Soc. 1999; 121:7090.
82. Boyd PDW, Hodgson MC, Rickard CEF, Oliver AG, Chaker L, Brothers PJ, Bolkskar RD, Tham FS, Reed CA. J. Am. Chem. Soc. 1999; 121:10487.
83. Rodriguez J, Kirmaier C, Holten D. J. Am. Chem. Soc. 1989; 111:6500.
84. Brun AM, Harriman A, Heitz V, Sauvage J-P. J. Am. Chem. Soc. 1991; 113:8657. (and references therein).
85. The incomplete quenching (0.5 versus 2.3 ns) is attributed to competition between intersystem crossing and energy transfer that generates the MLCT excited state of the [Cu(phen)₂]⁺ complex.
86. It should be noted that both kinetic traces have a minor ultrafast component about 1 ps, which is due to rapid deactivation through internal conversion from the porphyrin S₂ to the S₁ states or solvent reorganization.
87. Ruthkosky M, Kelly CA, Castellano FN, Meyer GJ. Coord. Chem. Rev. 1998; 171:309.
88. Scaltrito DV, Thompson DW, O'Callaghan JA, Meyer GJ. Coord. Chem. Rev. 2000; 208:243.

**Figure 1.**

Structures of (ZnP)₂-rotaxane-C₆₀ **1** and the related ZnP-[2]catenate-C₆₀ **2** ($\text{Ar} = 3,5\text{-di-}tert\text{-butylphenyl}$) and computational models showing their folded and stretched conformations, respectively. In the case of rotaxane **1**, computational calculations were carried out with 3,5-di-*tert*-butylphenyl groups at the *meso* positions of the two ZnP groups, which were later removed for clarity of presentation.

**Figure 2.**

Structures of (ZnP)₂-catenate-C₆₀ **3** derived from complexation of DABCO with the ZnP groups of rotaxane **1** and a Cu-free (ZnP)₂-rotaxane-C₆₀ **4**. Ar = 3,5-di-*tert*-butylphenyl.

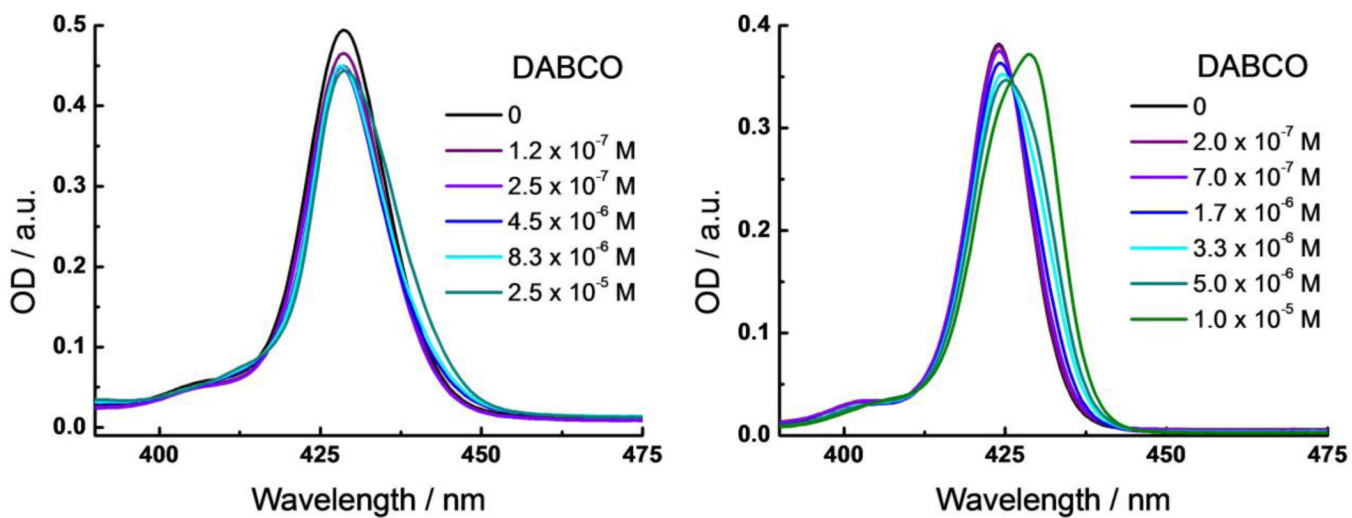
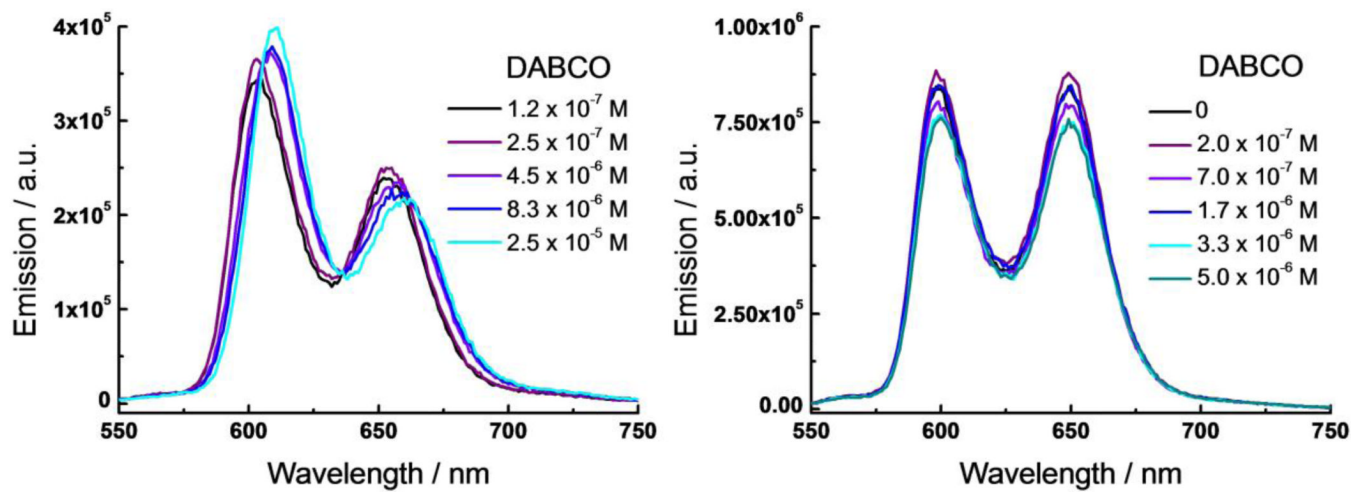
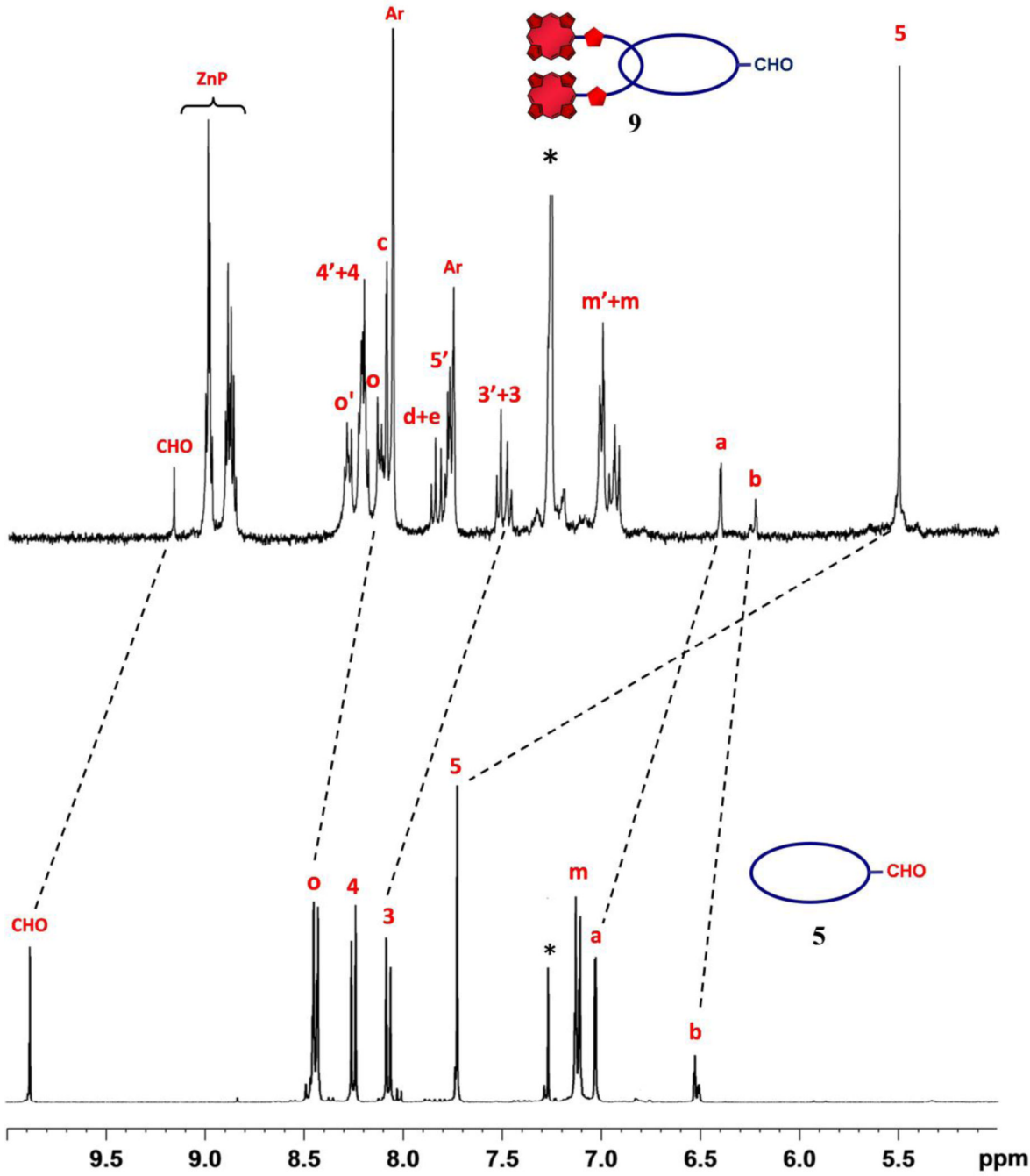


Figure 3.

UV-Vis absorption spectra of rotaxane **1** (1.0 × 10⁻⁶ M), left, and ZnTPP reference, right, upon titration with DABCO (from 0 to 1.0 or 2.5 × 10⁻⁵ M) in anisole at 25 °C. a.u. = arbitrary unit.

**Figure 4.**

Emission spectra of **1** (1.0×10^{-6} M), left, and of ZnTPP reference, right, upon titration with DABCO (from 0 to 1.0 or 2.5×10^{-5} M) in anisole at 25°C . Excitation wavelength for **1** and ZnTPP reference was 421 nm and 415 nm, respectively. Emissions were corrected in both cases with respect to the absorption using equation $I = I_{\text{Obs}} / 1 - 10^{-A_{\text{ex}}}$.

**Figure 5.**

Partial ¹H NMR spectra of rotaxane **9** (top) and macrocycle **5** (bottom) (400 MHz, CDCl₃ 298K). For lettering, see Scheme 1. The peak marked with an asterisk corresponds to residual CHCl₃.

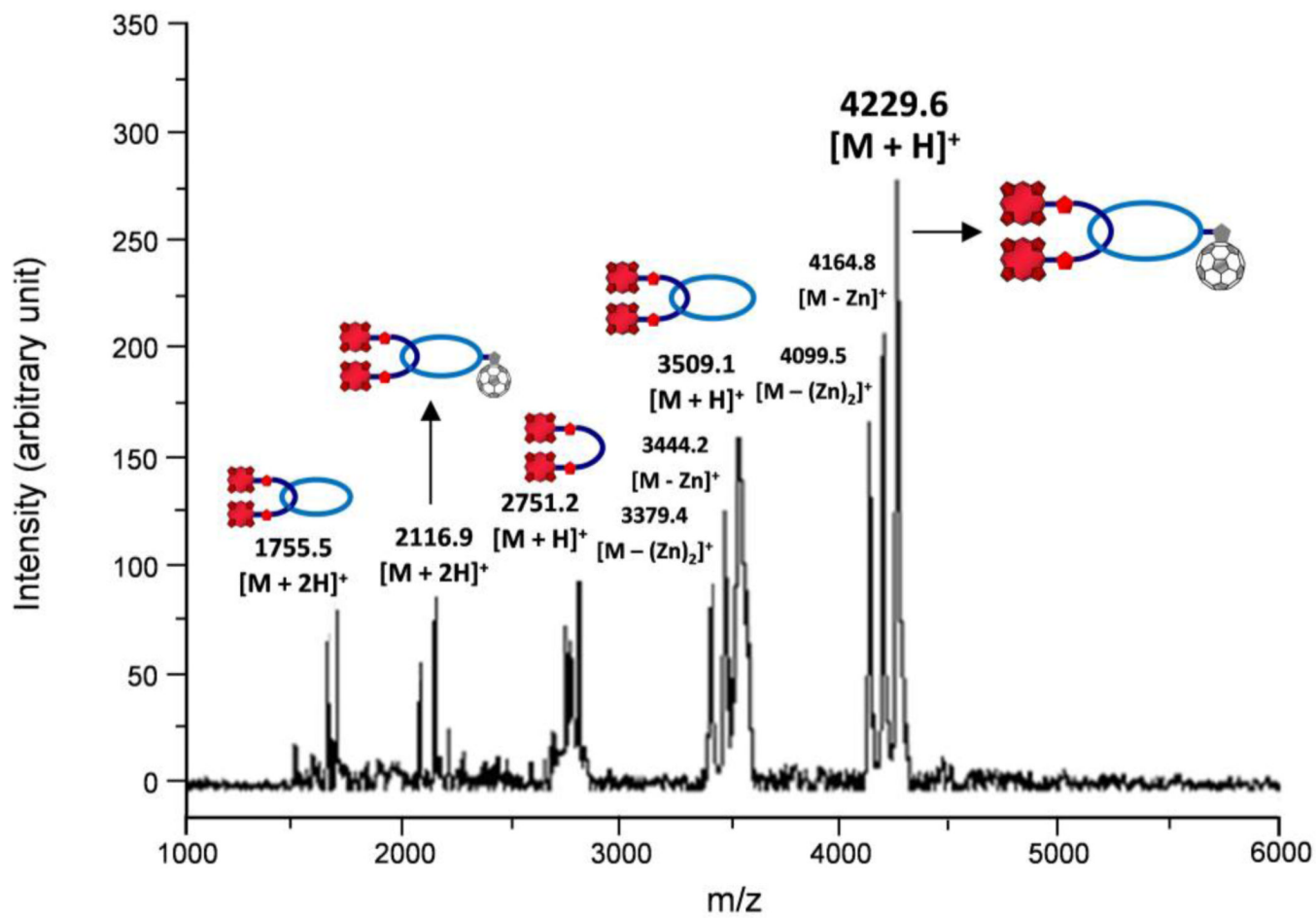


Figure 6.
MALDI-TOF spectrum (positive mode, α -cyano-4-hydroxycinnamic acid matrix) of rotaxane **4**. Loss of zinc ion from the porphyrin components is observed in the spectrum due to addition of trifluoroacetic acid (TFA), needed to induce ionization for MALDI-TOF detection.

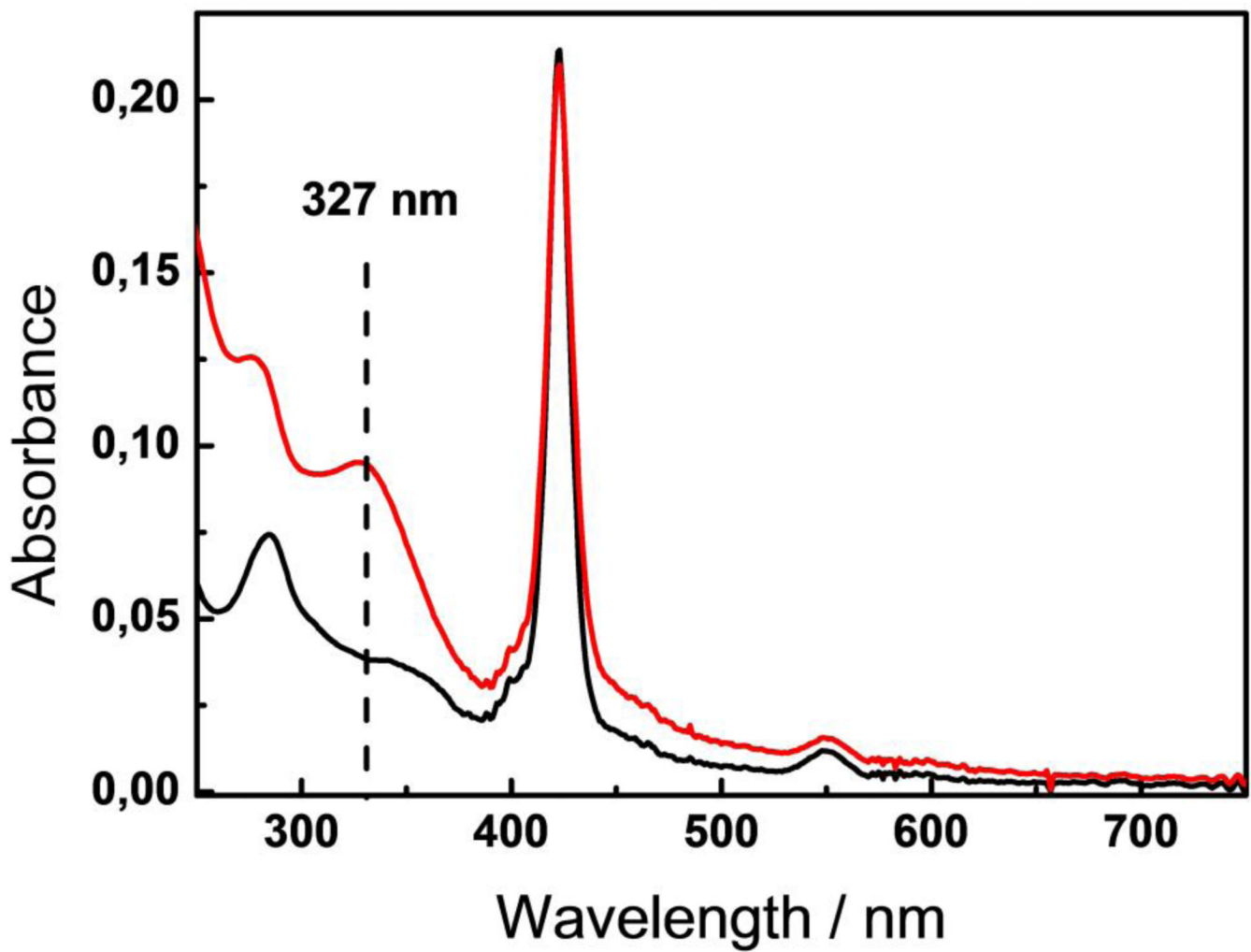


Figure 7.
UV-Vis absorption spectra of ZnP-rotaxane-benzaldehyde precursor **9** (black) and (ZnP)₂-rotaxane-C₆₀ **4** (red) (10^{-6} M, dichloromethane, 25°C). The stronger absorption of **4** at 327 nm attests to the successful introduction of C₆₀ to the rotaxane structure through a Prato reaction. a.u. = arbitrary units.

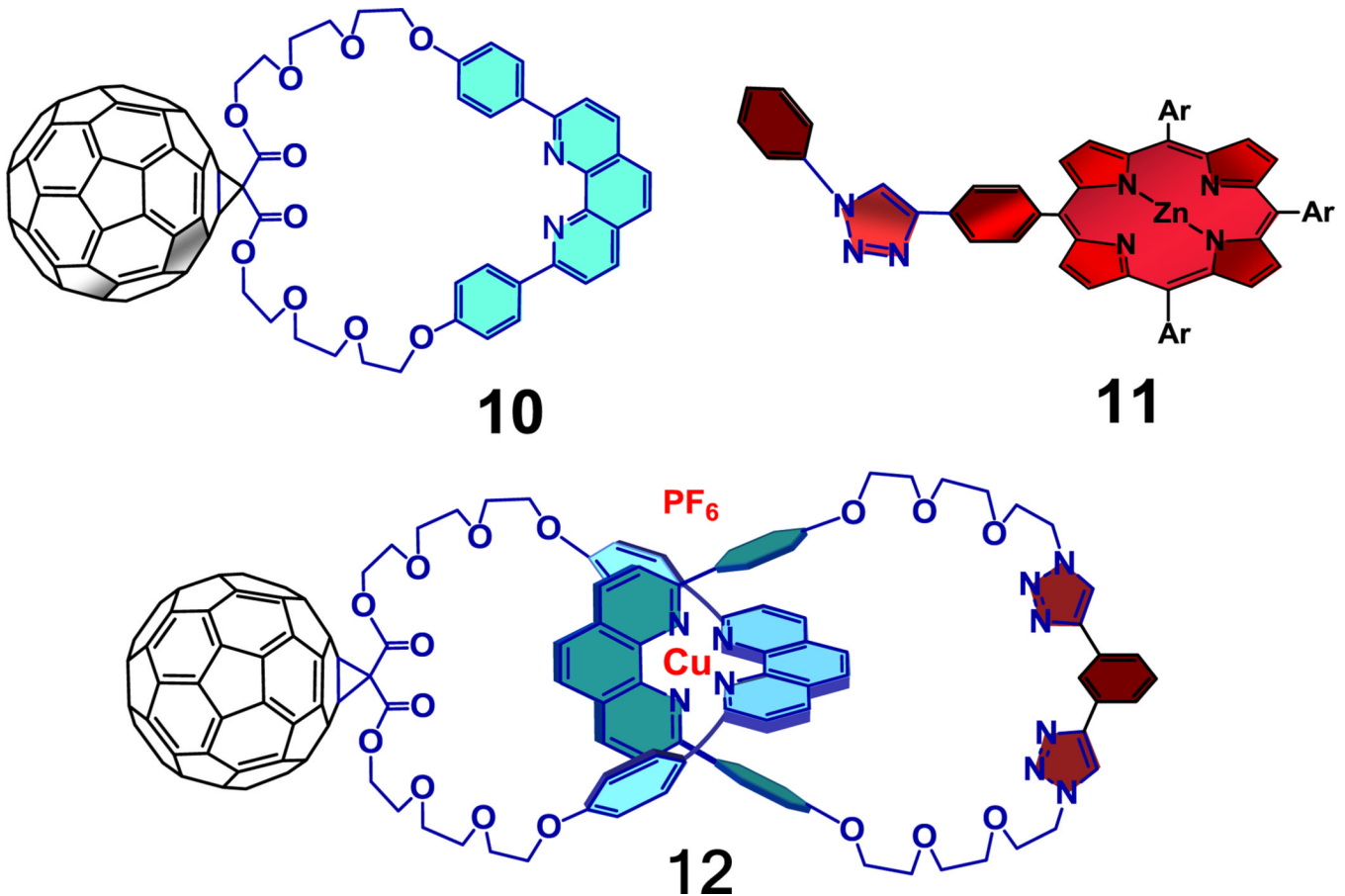


Figure 8.

References and model compounds studied by transient absorption techniques in the present work.

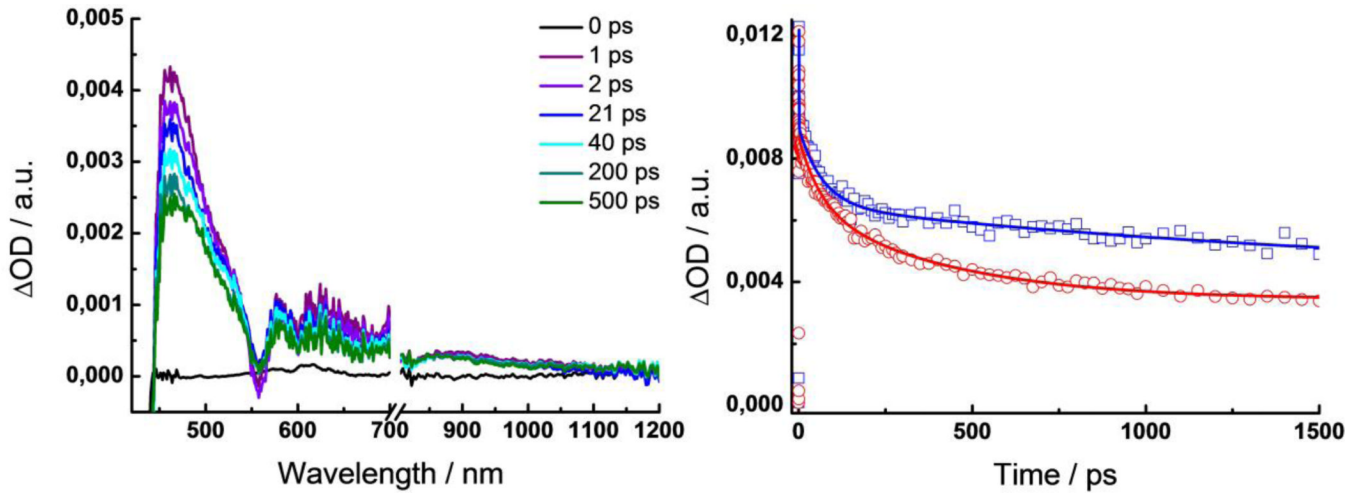


Figure 9.

Left: Differential absorption spectra obtained upon excitation of rotaxane **8** at 424 nm in anisole with time delays between 0 and 500 ps at room temperature. Right: Time absorption profiles in anisole at 460 nm for rotaxane **8** (blue squares) and rotaxane **1** (red circles), monitoring deactivation of ZnP singlet excited states. a.u. = arbitrary units.

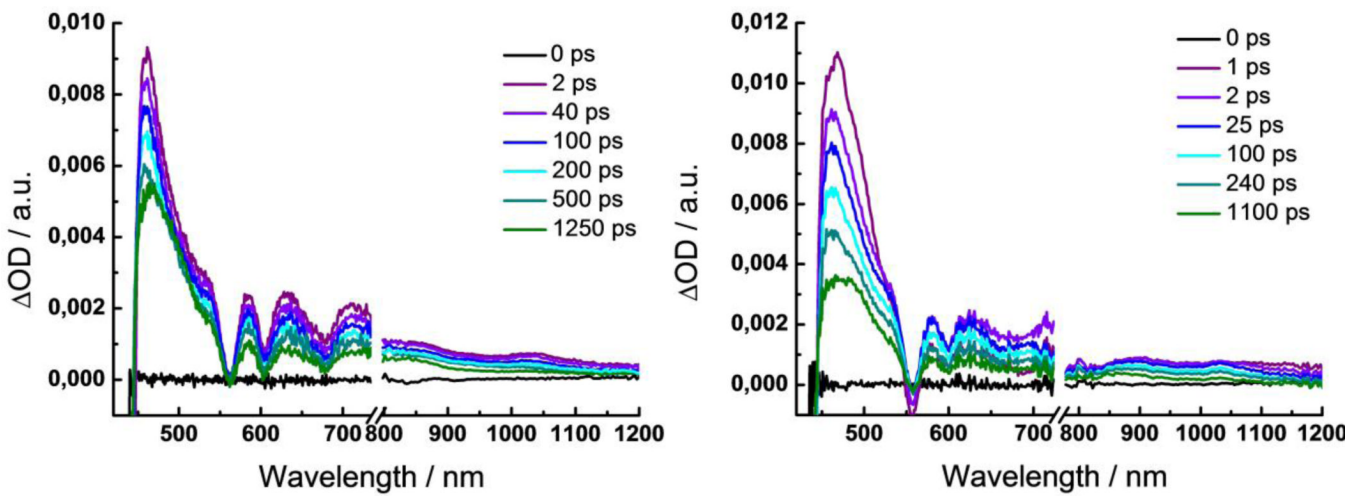
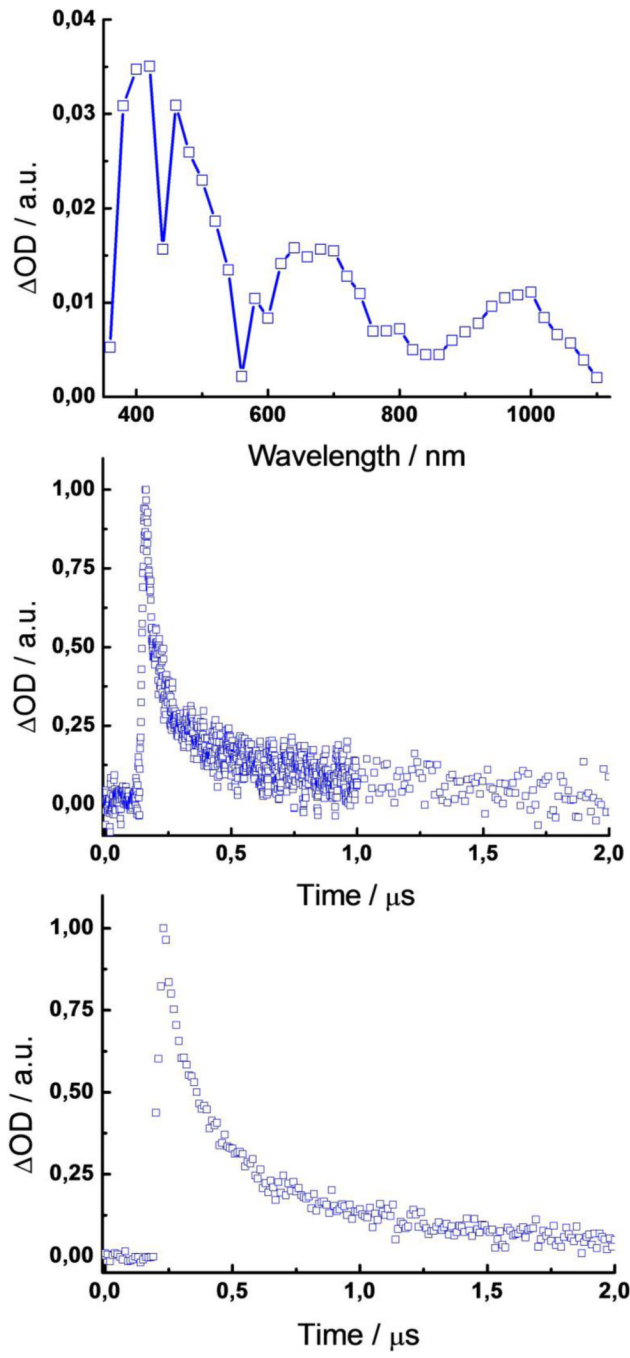
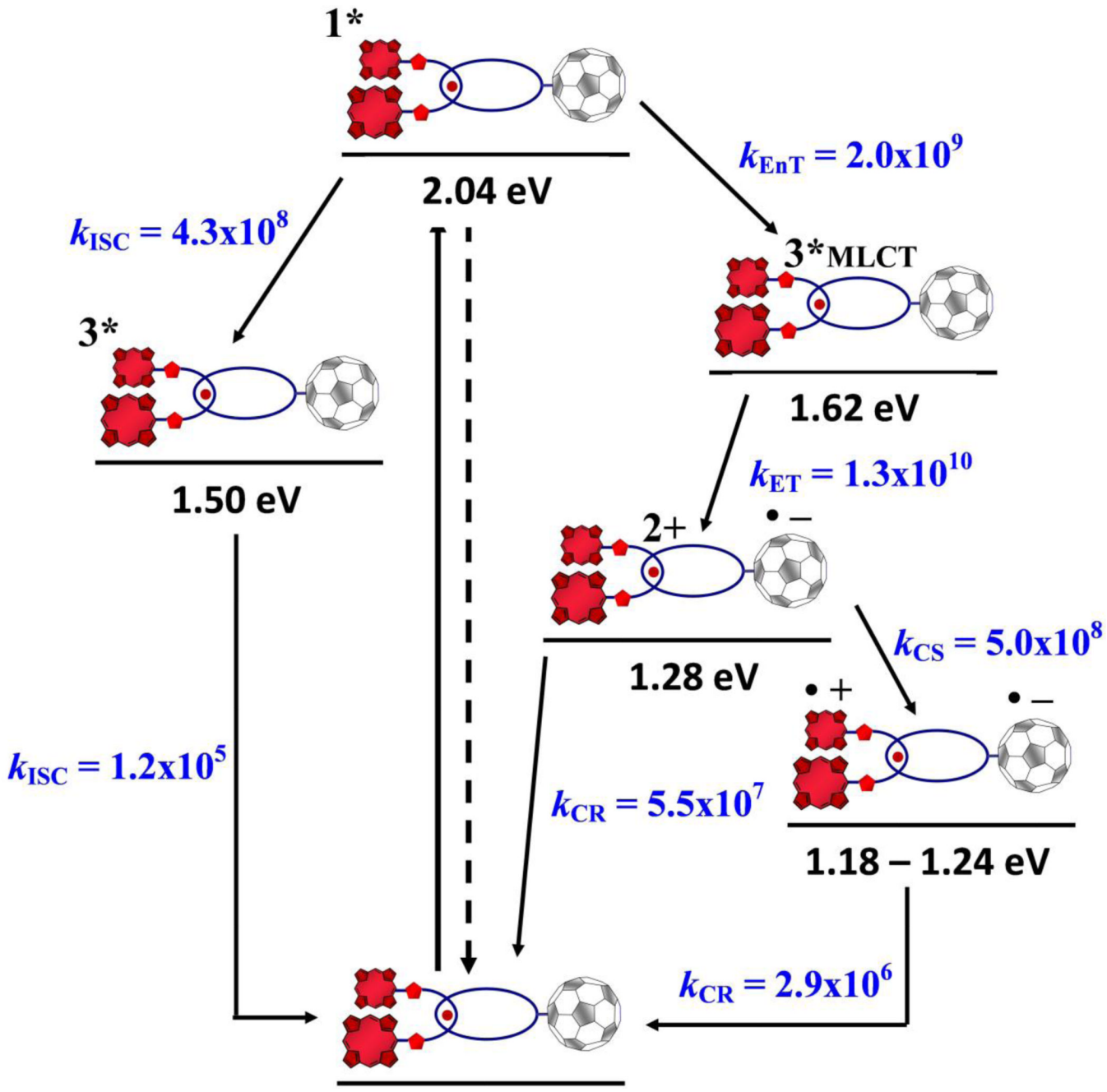


Figure 10.

Differential absorption spectra obtained upon excitation of rotaxane **1** at 424 nm in PhCN (left) and anisole (right) at room temperature with time delays between 0 and 1250 ps.

**Figure 11.**

Top: Differential absorption spectrum (visible and NIR range) obtained 165 ns after the laser pulse upon nanosecond flash photolysis (355 nm) of **1** in anisole at room temperature.
Middle: time absorption profile at 1020 nm, monitoring the charge recombination process.
Bottom: time absorption profile at 660 nm, monitoring the charge recombination process.
a.u. = arbitrary units.

**Figure 12.**

Energy level diagram, proposed decay pathways, and rate constants in s^{-1} for rotaxane **1** following excitation at the *Soret* band (424 nm) in PhCN. The positive charge of the $[\text{Cu}(\text{phen})_2]^+$ complex in the ground state is not displayed in the energy diagram. k_{EnT} = rate constant for energy transfer; k_{ET} = rate constant for electron transfer; k_{CS} = rate constant for the charge shift; k_{CR} = rate constant for charge recombination, and k_{ISC} = rate constant for intersystem crossing.

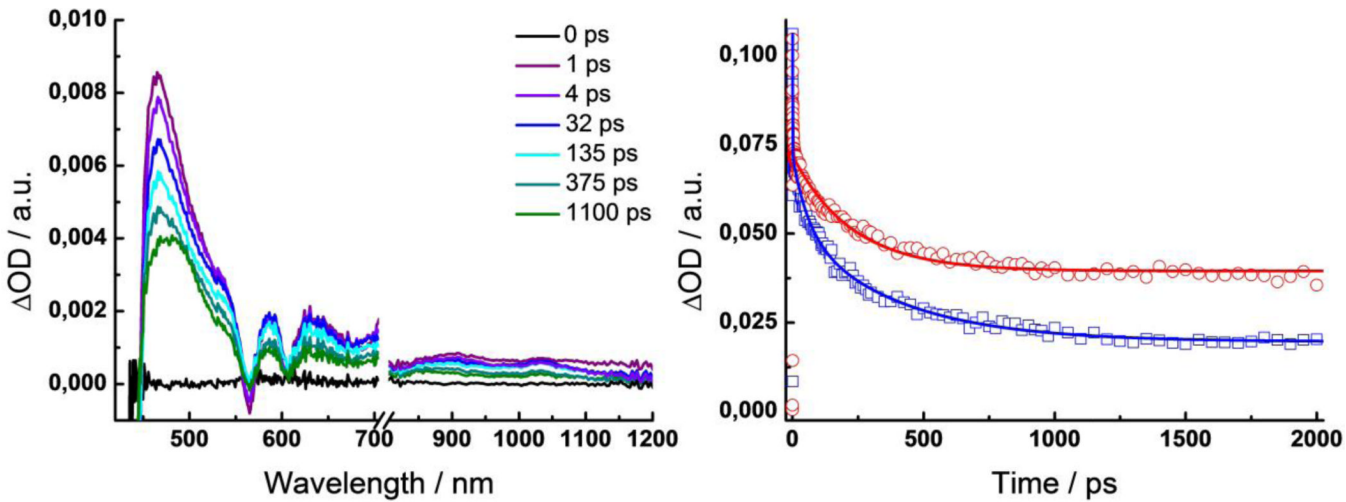
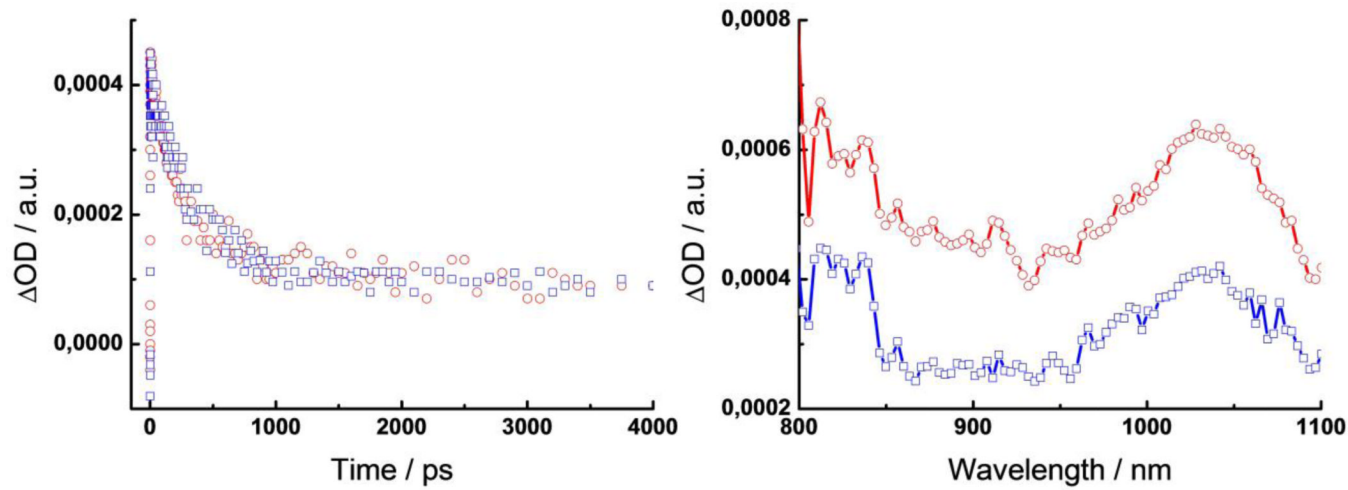


Figure 13.

Left: differential absorption spectra (visible range) obtained upon 424 nm excitation of **3** with DABCO (1:5) in anisole with time delays between 0 and 1100 ps at room temperature.
Right: time-absorption profiles of the spectrum at 460 nm (monitoring ${}^1\text{ZnP}^*$ species) in the absence (**1**, blue squares) and presence (**3**, red circles) of DABCO.

**Figure 14.**

Left: time/absorption profiles at 920 nm upon 387 nm femtosecond excitation of rotaxane **1** (red circles) and rotaxane **3** (1:5 rotaxane DABCO) (blue squares) in anisole, monitoring the deactivation of the C₆₀ singlet excited state. Right: differential absorption spectra (NIR range) obtained upon 387 nm excitation of **1** (red circles) and **3** (1:5 rotaxane DABCO) (blue squares) in anisole with time delays of 5 ps at room temperature.

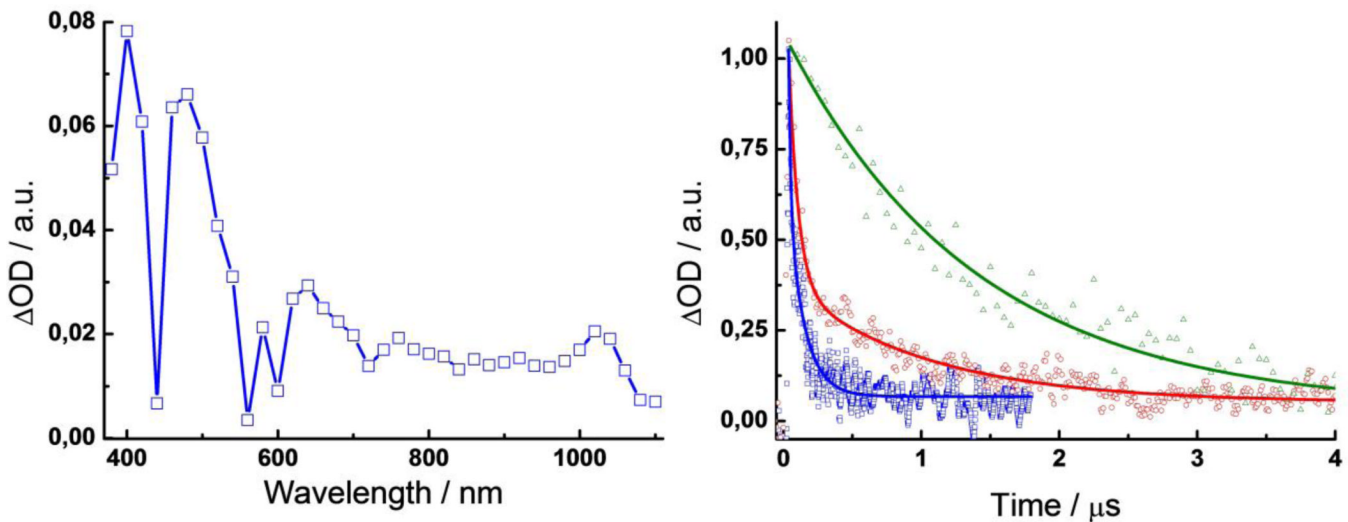
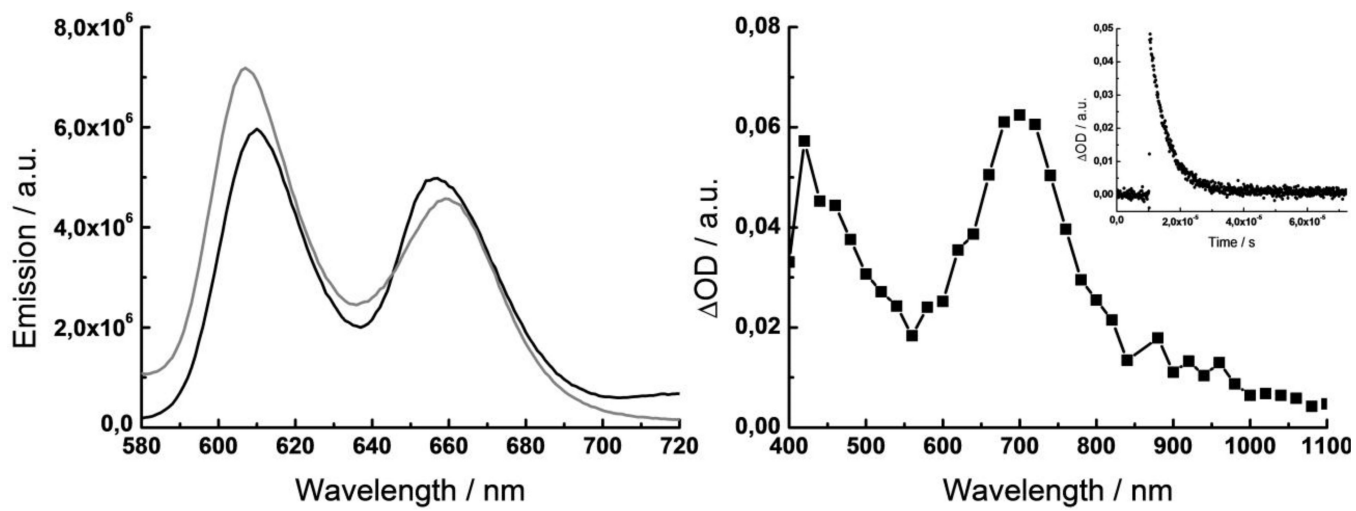
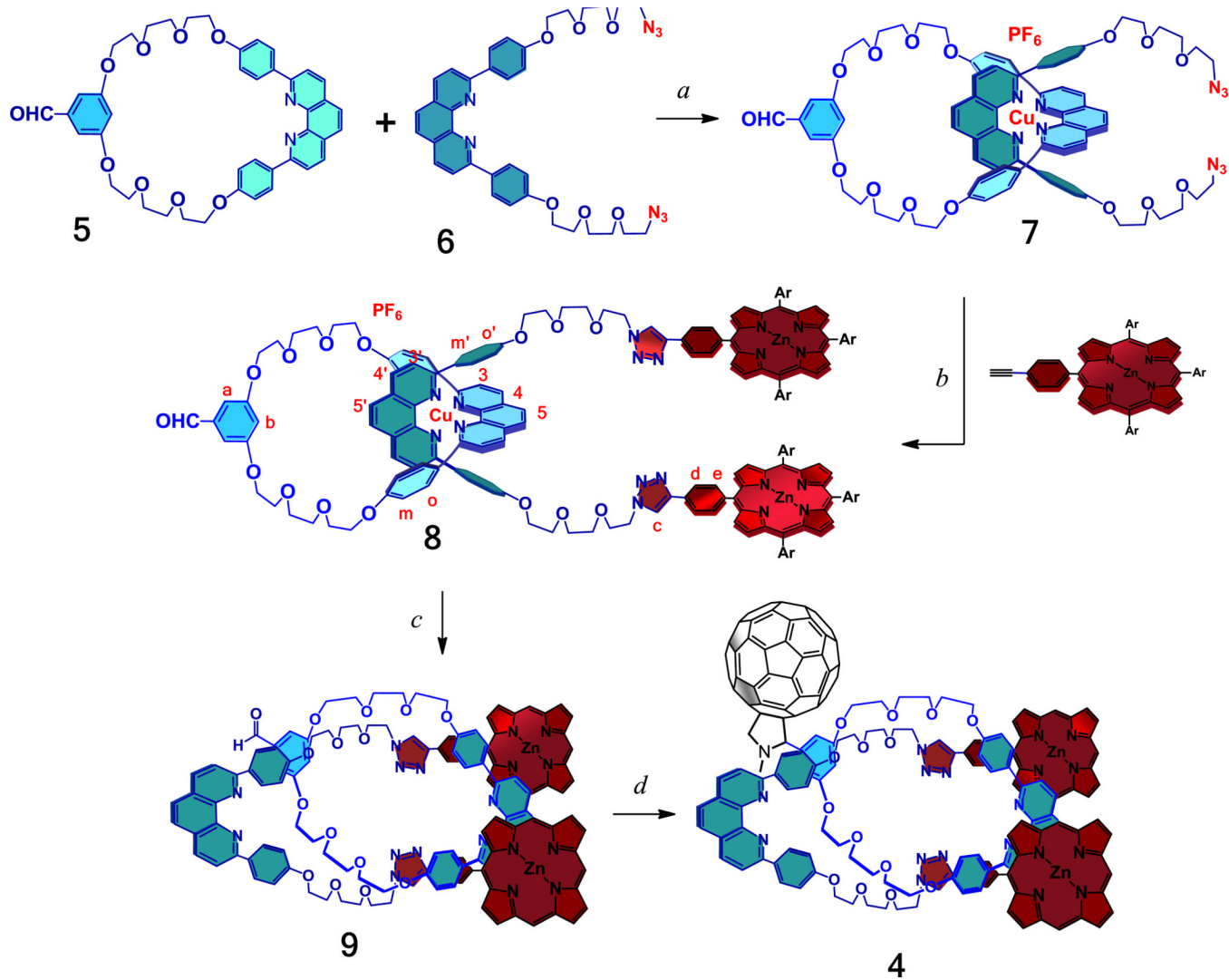


Figure 15.

Left: differential absorption spectrum (visible and NIR range) obtained upon nanosecond flash photolysis (355 nm) of **3** in anisole at 85 ns after the laser pulse at room temperature. Right: time profiles of the spectrum at 1020 nm in the absence (**1**, blue squares) and presence (**3**, red circles = 1020 nm; green triangles = 660 nm) of DABCO. a.u. = arbitrary units.

**Figure 16.**

Left: Emission spectra upon 429 nm excitation of dilute PhCN solutions of ZnP reference **11** (1.0×10^{-6} M – black spectrum) and of Cu-free rotaxane **4** (1.0×10^{-6} M – grey spectrum). The optical density at the 429 nm excitation wavelength was 0.35. Right: differential absorption spectrum (visible and NIR range) observed following nanosecond flash photolysis (355 nm) of **4** in benzonitrile at room temperature 80 ns after the laser pulse; Inset: time profile at 700 nm, monitoring triplet excited state decay. a.u. = arbitrary units.

**Scheme 1.**

Synthetic route to Cu-free (ZnP)₂-rotaxane-C₆₀ **4** ($\text{Ar} = 3,5\text{-di-}tert\text{-butylphenyl}$, present at the *meso* positions of the ZnP moieties in rotaxanes **4** and **9** but not shown for reasons of clarity). *a*) $[\text{Cu}(\text{CH}_3\text{CN})_4]\text{PF}_6$, $\text{CH}_2\text{Cl}_2/\text{CH}_3\text{CN}$, rt, 3 h, quantitative; *b*) CuI, sodium ascorbate, sulfonated bathophenanthroline, DBU, $\text{H}_2\text{O}/\text{EtOH}$, rt, 12 h, 65 % yield; *c*) KCN, $\text{CH}_2\text{Cl}_2/\text{CH}_3\text{CN}$, rt, 4 h, quantitative; *d*) C_{60} , sarcosine, toluene, reflux, 6 h, 13 % yield.